Fault facies and its application to sandstone reservoirs

Alvar Braathen, Jan Tveranger, Haakon Fossen, Tore Skar, Nestor Cardozo, S. E. Semshaug, Eivind Bastesen, and Einar Sverdrup

ABSTRACT

The concept of fault facies is a novel approach to fault description adapted to three-dimensional reservoir modeling purposes. Faults are considered strained volumes of rock, defining a three-dimensional fault envelope in which host-rock structures and petrophysical properties are altered by tectonic deformation. The fault envelope consists of a varying number of discrete fault facies originating from the host rock and organized spatially according to strain distribution and displacement gradients. Fault facies are related to field data on dimensions, geometry, internal structure, petrophysical properties, and spatial distribution of fault elements, facilitating pattern recognition and statistical analysis for generic modeling purposes. Fault facies can be organized hierarchically and scale independent as architectural elements, facies associations, and individual facies. Adding volumetric fault-zone grids populated with fault facies to reservoir models allows realistic fault-zone structures and properties to be included.

To show the strength of the fault-facies concept, we present analyses of 26 fault cores in sandstone reservoirs of western Sinai (Egypt). These faults all consist of discrete structures, membranes, and lenses. Measured core widths show a close correlation to fault displacement; however, no link to the distribution of fault facies exists. The fault cores are bound by slip surfaces on the hanging-wall side, in some cases paired with slip surfaces on the footwall side. The slip surfaces tend to be continuous and parallel to the fault core at the scale of the exposure. Membranes are continuous to semicontinuous, long and thin layers of fault rock, such as sand gouge, shale gouge, and breccia, with a length/thickness ratio that exceeds 100:1. Most

AUTHORS

ALVAR BRAATHEN ~ Center for Integrated Petroleum Research and Department of Earth Science, University of Bergen, 5020 Bergen, Norway; present address: University Center in Svalbard, Norway; alvar.braathen@unis.no

Alvar Braathen is a professor in structural geology at the University Center in Svalbard and an adjunct professor at the Department of Earth Science, University of Bergen. He received his M.S. degree and his Ph.D. from the University of Tromsø, Norway. His research covers aspects of fold and thrust belts and extensional tectonics, with a current focus on fault description and the importance of faults for fluid flow.

JAN TVERANGER ~ Center for Integrated Petroleum Research, University of Bergen, 5020 Bergen, Norway

After receiving his Doctor of Science title from the University of Bergen, Jan Tveranger worked as a polar Quaternary scientist for several years before being engaged by Saga Petroleum and subsequently Norsk Hydro as a reservoir geologist. He is currently employed as a senior researcher and research coordinator at the Center for Integrated Petroleum Research, University of Bergen, focusing on description and modeling of reservoir properties of faults and paleokarst features.

HAAKON FOSSEN ~ Center for Integrated Petroleum Research and Department of Earth Science, University of Bergen, Norway

Haakon Fossen received his Ph.D. from the University of Minnesota in 1992. He joined Statoil in 1986 and, since 1996, has been a professor in structural geology at the University of Bergen. His scientific interests cover the evolution and collapse of mountain ranges, the structure of rift basins, and petroleum-related deformation structures at various scales, with current focus on deformation bands and subseismic faults.

TORE SKAR ~ StatoilHydro ASA, Stavanger, Norway

Tore Skar received his M.S. degree and Ph.D. in geology from universities in Bergen and Amsterdam. After some years as a senior researcher at the University of Bergen, he moved to the senior geologist position in StatoilHydro. His scientific interests cover sedimentology and structural geology.

NESTOR CARDOZO ~ Department of Petroleum Engineering, University of Stavanger, 4036 Stavanger, Norway

Nestor Cardozo received his B.S. degree in geology from the Universidad Nacional de Colombia in

1994 and his Ph.D. in geology from Cornell University in 2003. He is an associate professor at the University of Stavanger. His scientific interests cover faults, their related deformation, and their implementation in reservoir models.

S. E. SEMSHAUG ~ *Center for Integrated Petroleum Research and Department of Earth Science, University of Bergen, 5020 Bergen, Norway*

Siv Semshaug works as an exploration geologist in rock source in Bergen. In parallel, she is undertaking her Ph.D. through the Center for Integrated Petroleum Research, University of Bergen. She also received her M.S. degree in structural geology from the same university. Her current research focuses on fault siliciclastic rocks and their importance for reservoir performance.

EIVIND BASTESEN ~ *Center for Integrated Petroleum Research and Department of Earth Science, University of Bergen, Norway*

Eivind Bastesen is a Ph.D. student at the Center for Integrated Petroleum Research at the University of Bergen. He also received his M.S. degree in structural geology from the same university. His current research interests are extensional faults in carbonates and siliciclastic rocks, with a focus on field descriptions and quantification of fault zones.

EINAR SVERDRUP ~ *Dana Petroleum Norway AS, P.O. Box 128, N-1325 Lysaker, Norway*

Einar Sverdrup is the exploration manager of Dana Petroleum Norway. He received his M.S. degree and Ph.D. degrees from the University of Oslo, Norway. His research topics cover sedimentology and diagenesis, fault properties, and flow characterization of seismic to subseismic reservoir heterogeneities.

observed lenses are four sided (Riedel classification of marginal structures) and show open to dense networks of internal structures, many of which have an extensional shear (R) orientation. The average lens long axis/short axis aspect ratio is about 9:1.

INTRODUCTION

Faults can be pathways or obstacles to fluid flow in the crust (Chester et al., 1993; Caine et al., 1996; Seront et al., 1998; Manzocchi et al., 1999, 2008), and as such they have received significant attention (e.g., Koestler and Hunsdale, 2002; Boult and Kaldi, 2005; Sorkhabi and Tsuji, 2005). Their influence on fluid flow is determined by the spatial distribution of flow-related petrophysical properties within the host-rock volume affected by tectonic deformation, i.e., the fault envelope (Tveranger et al., 2005). Describing fault properties in a realistic way therefore requires a method where faults are envisaged as volumetric entities composed of distinct, structural elements with distinct physical characteristics and spatial distributions on a given scale of observation. We introduce here the concept of fault facies as a way to describe and organize structural elements of the fault-strain envelope.

Facies Concept in Earth Sciences

The concept of facies (Steno, 1671; Gressly, 1838; Teichert, 1958) has traditionally been applied to descriptions of sedimentary (Reading, 1986) and metamorphic rocks (Winkler, 1976) and, to a lesser extent, to ductilely deformed rocks (Hansen, 1951; Tikoff and Fossen, 1999). This concept has also been applied to geochemistry (Ernst, 1970), interpretation of well logs (i.e., Rider, 1996), and seismic character (Mitchum et al., 1977). In general, a facies can be defined as "a body of rock with specific characteristics" (Middleton, 1978, p. 4). Ideally, it should be a distinctive rock that forms under certain conditions, reflecting a particular process or environment. The main strength of the facies approach lies in its flexibility for subdividing bodies of rock into distinct classes or groups at any scale according to a specific set of properties or features, observed or interpreted. This makes facies a powerful tool for pattern recognition, description, modeling, and forecasting of property distributions in the subsurface. The introduction of fault facies is a natural extension of the facies concept into the realm of faulted rock bodies. We define a fault facies as "any feature or rock body that has properties derived from tectonic deformation" (Tveranger et al., 2005, p. 68). Similar to sedimentary

facies, individual fault facies occur in certain combinations, or associations; in transitional sequences, or successions; and in larger scale associations with volumetric dimensions, the architectural element.

Faults in Reservoir Models

Reservoir models have progressively become more sophisticated with the rapid development of CPU power and three-dimensional (3-D) computer graphics. Present-day geomodeling tools can provide multimillion-cell stochastic realizations that incorporate depositional architectures and properties as well as uncertainties attached to these in high detail. These models serve as input to fluid-flow simulators used to forecast reservoir behavior for exploration and production purposes. However, conventional reservoir modeling tools include faults in a highly simplified way using a combination of offsets along grid splits and calculated transmissibility multipliers to capture fault impact on fluid flow across faults (Walsh et al., 1998; Manzocchi et al., 1999; Manzocchi et al., 2008). Known and important features of reservoir behavior, such as fluid flow inside the fault envelope, can thus not be included explicitly, and flow between nonjuxtaposed cells can only be included in an ad-hoc fashion using history matching. This renders fault description as implemented in present-day simulators inadequate for detailed evaluation and forecasting of fault sealing and compartmentalization. Furthermore, not including the fault envelope as a volumetric entity with altered porosity relative to the surrounding host rock may lead to the overestimation of in-place volumes. Finally, the lack of explicit descriptions of fault envelopes in current models renders them unsuitable as tools for detailed planning and risk assessment prior to drilling through faults.

Including fault envelopes as explicit volumetric grids populated by products of the faulting process offers an alternative way for handling fault properties in reservoir models. Recent research (Syversveen et al., 2006; Fredman et al., 2007, 2008; Soleng et al., 2007) has studied the feasibility of this approach using a range of synthetic geological data sets to develop a technical framework for fault-zone modeling. By introducing volumetric fault zones into standard reservoir models and supplying appropriate conditioning parameters for fault-envelope structure and strain distribution, fault facies can be handled using existing modeling tools developed for sedimentary facies. The availability of a technical framework and workflows allowing explicit representation of fault features as facies focuses the attention toward how fault facies should be described and organized in the field. Below we present the use of fault-facies classification schemes, which allow systematic observation and quantification of fault-zone elements for 3-D modeling purposes.

FAULT DESCRIPTIONS

Faults and Structural Elements

Faults appear in all tectonic settings. Accordingly, faults can be ascribed to a fault regime (Figure 1). A fault system consists of isolated faults or fault arrays (e.g., Walsh et al., 2003), each with a distinct geometry (planar, listric, ramp-flat-ramp, etc.), dimension (length, width, height), and sense of slip (normal, reverse, strike-slip). Individual faults are contained within fault-strain envelopes, within which the initial rock properties have been modified. Fault envelopes may overlap in space, as seen in relay zones between interacting splay faults in a fault array (Huggins et al., 1995; Walsh et al., 2003; Rotevatn et al., 2007). Most fault envelopes exhibit a fault-parallel zonation, where elements such as the fault core, damage zones, and drag zones are first-order zonal features (Chester et al., 1993; Caine et al., 1996; Burhannudinnur and Morely, 1997; Childs et al., 1997; Heynekamp et al., 1999; Braathen et al., 2004, Collettini and Holdsworth, 2004; Myers and Aydin, 2004; Berg and Skar, 2005; Van der Zee and Urai, 2005; Childs et al., 2009). The main structural elements within a typical fault envelope are (Figure 2): (1) fault-rock layers or pockets, (2) lenses, (3) slip surfaces, (4) shear fractures (small-scale slip surfaces), (5) extension fractures, (6) deformation bands, and (7) contractional features such as cleavages and stylolites. We
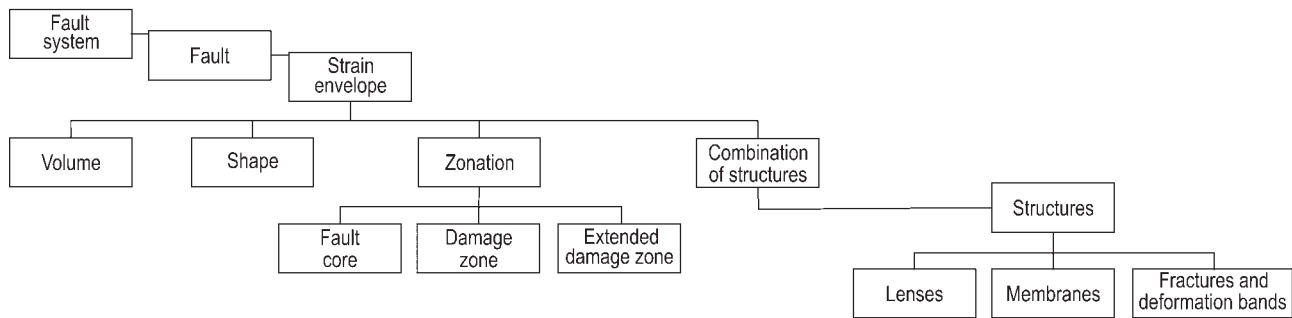
Fault description scheme

Figure 1. Fault-facies hierarchical classification scheme. Faults can be ascribed to a fault system that consists of isolated faults or fault arrays with a distinct geometry (planar, listric, ramp-flat-ramp), dimension (length, width, height), and sense of slip (normal, reverse, strike slip). Individual faults are contained within strain envelopes that exhibit a given volume and shape as well as a fault-parallel zonation, where elements such as the fault core, brittle damage zones, and ductile drag zones or extended damage zones are first-order zonal features or architectural elements. Each of these major elements is composed of combinations of structures, such as discrete structures (fractures and deformation bands), membranes, and lenses, which can be ascribed to facies associations and facies.

will return to the description and classification of these elements below.

All structural elements mentioned above are found in faults observed in the field, although rarely as isolated features allowing simple interpretations. Faults commonly affect a significant volume of the surrounding host rock in the shape of a fault envelope, consisting of one or more major strands, and several subsidiary faults and discrete structures (e.g., Childs et al., 1997; Myers and Aydin, 2004; Berg and Øian, 2007). Our ability to study faults in outcrop is limited by the fact that they commonly constitute weak zones in the rock covered by surficial debris and vegetation. Outcrops commonly only display a two-dimensional (2-D) view of the fault envelope, and cases where faults can be studied in successive cliffs along a meandering valley or canyon, opening for a 3-D analysis, are few. Fault envelopes can rarely be studied in true 3-D, with a few exceptions related to quarry and tunnel systems (e.g., Wallace and Morris, 1986; Huggins et al., 1995; Kristensen et al., 2008).

Fault Facies and Their Classifications

In the analysis of faults in outcrops, as presented above and also discussed in the literature (Chester et al., 1993; Caine et al., 1996; Burhannudinnur and Morely, 1997; Childs et al., 1997; Heynekamp et al., 1999; Prestholm and Walderhaug, 2000; Braathen et al., 2004; Collettini and Holdsworth, 2004; Myers and Aydin, 2004; Van der Zee and Urai, 2005; Kristensen et al., 2008; Childs et al., 2009), obviously, many of the elements in faults are recurring, and therefore, they are globally representative for both sedimentary and crystalline rocks. On a general scale, the modification of initial host-rock properties within the fault envelope can be described in terms of the sum of properties of individual small-scale tectonic structures or combinations of such structures. To describe faults in more detail, the depiction of rock properties inside fault envelopes requires the identification and quantification of dimensions, geometry, and petrophysical properties of individual structural elements and element combinations present in the fault envelope, as well as their spatial patterns and distribution. Addressing several variables in faults systematically and independently of individual localities may serve as a guide toward organized data sets that are an essential input for facies analyses.

Similar to sedimentary facies, fault-facies definitions can be adapted in terms of scale and detail to the objective of the study and the data available. For example, deformation bands in porous sandstone can be defined as a fault facies. However, on the millimeter scale, deformation bands may have (1) an inner zone or core of intense shear-induced
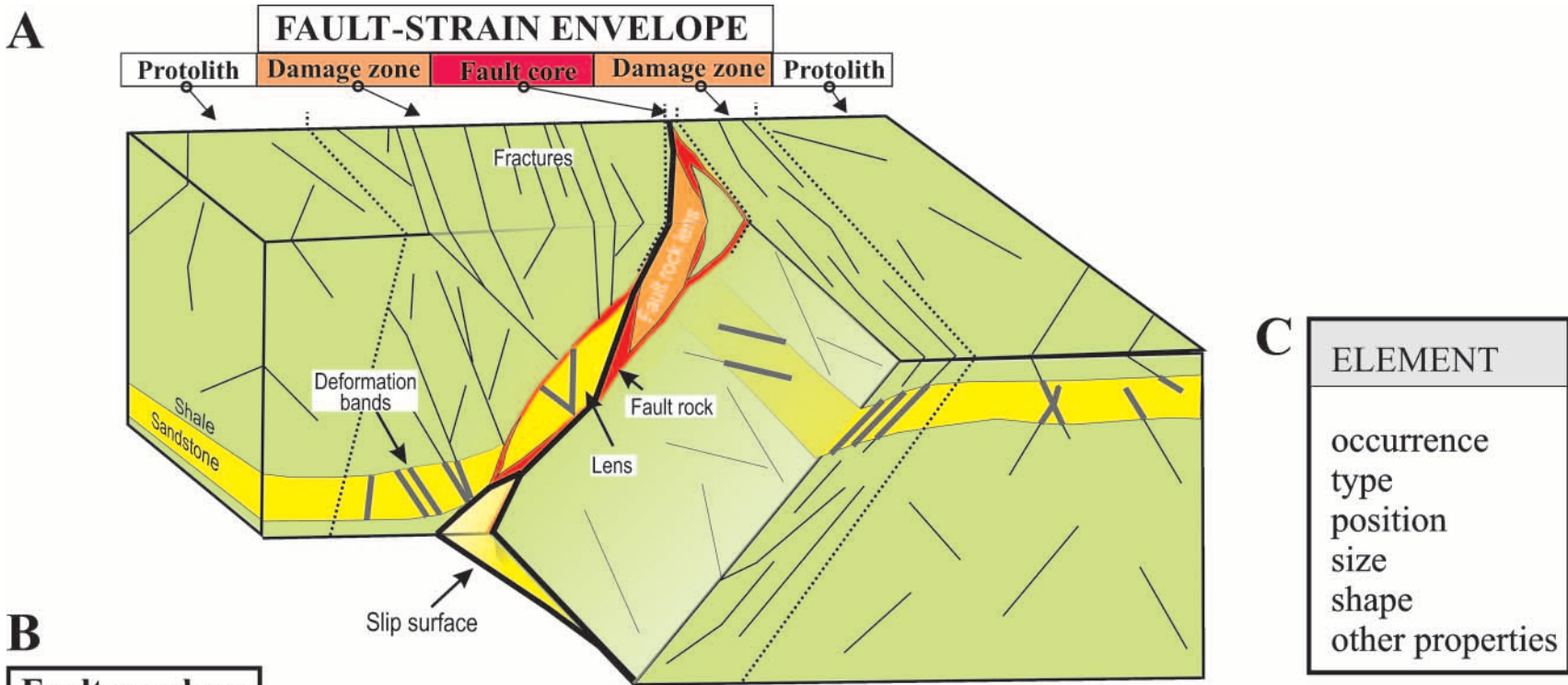
A

FAULT-STRAIN ENVELOPE

| Protolith | Damage zone | Fault core | Damage zone | Protolith |

Fractures

Fault rock lens

Deformation bands

Fault rock

Shale
Sandstone

Lens

Slip surface

C

ELEMENT

occurrence
type
position
size
shape
other properties

B

Fault envelope

STRAINED ROCK VOLUME	ZONING		APPEARANCE	TYPICAL ORIENTATION
	Fault core	**Damage zone**		
ELEMENTS	deformation band	deformation band	millimeter tabular zone	Riedel sets
	slip surface	slip surface	cohesion-free discontinuity	parallel with fault
	fracture	fracture	cohesion-free discontinuity	Riedel sets
	cleavage	cleavage	disolution and mineral orientation surface	parallel with fault or fold surface
	stylolith	stylolith	disolution surface	parallel with fault or fold surface
	fault-rock layer		deformed host-rock layer along fault	parallel with fault
	shale smear		smeared shale layer along fault	parallel with fault
	sand smear		smeared sand layer along fault	parallel with fault
	mixed unit	mixed unit	layer of mixed sand-shale	parallel with fault
	membrane		layer of fault rock or smear along fault	parallel with fault
	lens	lens	tectonic body of host or fault rock	long axis parallel with fault

BRAATHEN ET AL.

Figure 2. (A) Fault model showing common structures encountered in extensional fault envelopes in siliciclastic rocks. (B) Diagram presenting common descriptions used on elements in faults, as commonly reported in the literature. (C) Diagram illustrating parameters required as input to modeling of faults.

cataclasis and some compaction, (2) an enveloping zone of compaction and rare cataclasis, and sometimes (3) a central fracture that may or may not be mineral filled (Aydin, 1978; Gabrielsen et al., 1998; Fossen et al., 2007). Such deformation bands may thus be described as consisting of three fault facies, together defining a deformation-band fault-facies association. At outcrop scale, the deformation-band distribution in deformed sandstone may be subdivided into several shapes, for example open networks of deformation bands in a given sandstone layer. Such fault-facies associations can make up the architectural element damage zone.

Based on our outcrop observations of faults in porous sandstone, we divide the fault data sets into three main elements: (1) discrete structures, (2) membranes, and (3) lenses. In the following sections, structural elements of these groups and their facies classification are discussed before considering the importance of diagenesis in faults.

Discrete Structures

In faults (Figure 2), typical discrete structures, also called sharp discontinuities (without cohesion at time of development; Schultz and Fossen, 2008), are slip surfaces, shear fractures, extension fractures, and contractional features such as cleavages and stylolites. The cleavages and stylolites are controlled by the removal of material by dissolution processes (e.g., Groshong, 1975). All these elements are well described by, for example, Hancock (1985), Petit (1987), and Aydin (2000). Fractures exhibiting shear, such as slip surfaces, commonly have more or less continuous walls of deformed host rock, frequently seen as micrometer to millimeter lamina of cataclasite or gouge (Aydin and Johnson, 1983; Antonellini and Aydin, 1995; Shipton and Cowie, 2001; Shipton et al., 2005). Accordingly, slip surface(s) with deformed walls have been termed slip zones (e.g., Foxford et al., 1998). The slip surface is frequently seen to represent both the principal displacement (slip) surface in fault cores and fractures; the latter are hosted by individual deformation bands or deformation-band swarms (Aydin, 1978; Jamison and Stearns, 1982; Antonellini and Aydin, 1995; Shipton and Cowie, 2001; Fossen et al., 2007; Rotevatn et al., 2008).

Deformation bands are tabular strain-localization structures that form in highly porous rocks such as sandstone (Fossen et al., 2007), which also have been termed tabular discontinuities (Schultz and Fossen, 2008). Although deformation bands may take on a variety of kinematic modes, shear bands with some compaction are most commonly observed in naturally deformed porous sandstones. Deformation bands are generally stronger and more cohesive structures than fractures and show different petrophysical properties and displacement scaling relations (Fossen et al., 2007).

Extensional fault envelopes in porous sandstone commonly exhibit swarms, conjugate sets, anastomosing networks, or individual deformation bands (e.g., Aydin, 1978; Hesthammer and Fossen, 2001; Shipton and Cowie, 2001; Berg and Skar, 2005), which can be classified according to type and shape (Figure 3). Similar patterns are exhibited by fractures in nonporous or crystalline rocks (e.g., Chester et al., 1993; Caine et al., 1996). Each of the deformation-band expressions fills a certain rock volume, which can be described in terms of length, width, thickness, and shape. Each such rock volume has its characteristic deformational and thereby petrophysical properties that distinguish it from the surrounding volumes in the same fault envelope.

The shape of both fractures and deformation bands can be analyzed according to their orientation with respect to the main structure (Figure 3). Orientation analysis can follow the classifications introduced by Riedel (1929) (see also Logan et al., 1979; Katz et al., 2004), with extensional (R, x), isochoric (Y), and contractional (P, R') shear structures, or R, R', P, X, and Y shears, representing structural sets with given orientation and kinematics. As pointed out by Arboleya and Engelder (1995), the orientation of structures as they generate relates to the local stress field, which may rotate around faults, and as such could be different between the hierarchical orders of structures. This can contribute to a spread in orientations encountered in different shear (Riedel) structures.

Membranes

Basically, all faults, independent of throw and size, contain more or less persistent layers or membranes

Slip surface, fractures, and deformation bands (S)

A) Type (Ssl = slip surface, Sfr = fracture, Sdb = deformation band)

Sharp				Tabular
Fractures	FACIES			Deformation bands
	Ssl	Sfr	Sdb	
R	Ssl1	Sfr1	Sdb1	Extensional shear band
R'	Ssl2	Sfr2	Sdb2	
Y	Ssl3	Sfr3	Sdb3	Shear band
P	Ssl4	Sfr4	Sdb4	Contractional shear band
Joint	T	Sfr5	Sdb5	Dilation band
Solution surface	So	Sfr6	Sdb6	Compaction band

B) Shape (s)

FACIES	Single structure	Isolated network	Open network	Dense network	Anastomosing network	Swarm/Train
	Ss1	Ss2	Ss3	Ss4	Ss5	Ss6

Granular flow — A; Cataclasis — B; Fracture — C

Figure 3. Facies classification scheme for discrete structures, with types such as slip surface, fracture, and deformation bands. The classification is based on discrete structure types and their orientation as subsidiary structures, as discussed in the text. Shape relates to the appearance of individual or sets of structures, which can be connected to deformation style.

of rocks along the fault core. Several types of membranes are observed, spanning from cataclasites and breccias to fault gouge and smears (Figure 4). Whereas the cataclasites, breccias, and gouge are fault rocks that relate to the comminution of rocks (Sibson, 1977; Wise et al., 1984; Braathen et al., 2004), the smears are layers that are ductilely rotated and smeared along the fault core (e.g., Lehner and Pilaar, 1997; Yielding et al., 1997). Membranes are, for example, found along slip surfaces in porous sandstone as millimeter-wide cataclastic layers in the bounding wall rock (e.g., Foxford et al., 1998; Shipton and Cowie, 2001), or seen as shale gouge and sand gouge layers as described for the faults presented below, and in the literature (e.g., Burhannudinnur and Morely, 1997; Childs et al., 1997; Heynekamp et al., 1999; Prestholm and Walderhaug,

2000; Bense et al., 2003; Doughty, 2003; Myers and Aydin, 2004; Van der Zee and Urai, 2005; Rawling and Goodwin, 2006).

The shape of the membranes is of special interest because their common flow-retarding effect in connection with continuity is crucial for across-fault flow analysis (e.g., Færseth, 2006). Consequently, membrane analysis should establish continuity, herein spanning from continuous to pocket membranes (Figure 4B).

Lenses

Lenses are lozenge-shaped, tectonic rock bodies bound on all sides by slip surfaces and/or zones of concentrated shear, the latter commonly displaying membranes. Lenses consist of undeformed to strongly deformed host rock, or fault rock, as described by Lindanger et al. (2007) (see also Childs et al., 1996; Kristensen et al., 2008; Childs et al., 2009; Bastesen et al., 2009). Their location can be both in the core and the damage zone. However, herein we regard lenses as fault bodies that are not juxtaposed with their source layer, thus limiting their appearance to the fault core.

Lenses can be classified according to lithology, for example, sand, shale, a combination of sand and shale, or fault rocks (Figure 5). Most lenses show internal deformation, and as such can be described by a facies series spanning from undeformed to swarms of internal structures. Their shape is classified according to their boundaries through the identification of the structural orientations of their bounding margins. The terminology applied to the margin structures is that of the Riedel system discussed for discrete structures above. By combining such structures, possible shapes of lenses span from three sided (Ls3) to six sided (Ls6) and more (Bastesen et al., 2009).

Diagenesis in Faults

In many reservoirs, diagenesis in the low temperature realm of fault zones may govern fault-zone properties (e.g., Heynekamp et al., 1999; Bjørlykke et al., 2005), covering processes such as compaction, dissolution, recrystallization, and cementation. On a detailed level, such as for a given fault zone, the predictability of the effects caused by

Figure 4. Facies classification scheme of fault membranes (M). Membranes are layers of rock located along the fault core. Types include fault rocks, including gouge and smears, the latter related to ductile rotation and smearing or stretching of sedimentary layers along the fault. Membrane shapes describe the continuity of the layer in question.

A) Type (t), with Cement (-C)

	FACIES
Breccias (with clasts)	Mt1
Sand gouge	Mt2
Shale gouge	Mt3
Sand smear	Mt4
Shale smear	Mt5

B) Appearance / Shape (f, c)

Appearance	Continuity	%	Fault rock FACIES	Cement FACIES
Continuous		100	Mf1	Mc1
Semicontinuous		90–100	Mf2	Mc2
Ruptured		50–90	Mf3	Mc3
Patchy		10–50	Mf4	Mc4
Pocket		< 10	Mf5	Mc5

these processes is limited, particularly with respect to the presence and distribution of allogenic cements. However, cement seems most common in the more permeable units or structural elements, such as coarser sandstones and fractures. The latter are discussed by Laubach (2003), who presents a method that forecasts the propensity of fractures with respect to cement (see also Laubach and Ward, 2006). Furthermore, Heynekamp et al. (1999) reported calcite-cemented zones in and around the fault cores and established a tentative correlation between protolith grain size, deformation process, cementation, and permeability. For authigenic cement, recent developments in forecasting quartz dissolution and precipitation (Walderhaug, 1996; Walderhaug et al., 2001) can be applied to fault analysis. Examples of the latter include quartz cementation of deformation bands, as for example discussed by Hesthammer et al. (2002). Because this article focuses on structural elements, the secondary effects caused by diagenesis are superficially handled, as reflected by the fact that only distinct

cement occurrences are described as part of the membrane classes (Figure 4B). Less pervasive cement or cement as a diffuse mass or other diagenetic effects are not considered. An extension of the fault-facies concept should take diagenesis further into account.

ANALYSIS OF EXTENSIONAL FAULTS IN SANDSTONE

The attractiveness of fault-facies analysis lies in the systematic description of faults, which allows the comparison of observations of individual faults and analysis of fault data sets. To illustrate the value of fault-facies analysis, we present a data set consisting of 26 faults. To limit the scope, we here focus on the fault core.

All faults described here are located in western Sinai (Egypt), in the uplifted shoulder of the Suez rift (Figure 6; Table 1). Several major faults break the Sinai rift shoulder into major fault blocks, such as the Hammam-Faraun, Thal, and Baba faults (names from Sharp et al., 2000). For details on the geology of the area, see the works of Moustafa (1993), Sharp et al. (2000), Du Bernard et al. (2002), and Moustafa (2004). The sedimentary section of this region rests on the Pan-African basement and is commonly divided into lower prerift and upper synrift deposits (e.g., Moustafa, 2004). The lowermost pre-rift unit, the Cambrian to Cretaceous Nubian Sandstone, consists mainly of continental deposits. At the studied sites, deposits mainly consist of moderately lithified and porous, medium-grained fluvial and some eolian sediments. These units were buried to a maximum depth of 1500–2000 m (4921–6562 ft) at the onset of extensional rifting in the Suez rift (e.g., Sharp et al., 2000; Du Bernard et al., 2002; Moustafa, 2004). The following prerift Cretaceous to Eocene succession is generally distinguished by limestone and mudstone deposits, but it also hosts the Matulla Formation, consisting of porous shallow-marine sandstone of moderate grain size. The estimated burial depth for this unit at the start of rifting is approximately 800 m (2625 ft). An upper synrift section of Miocene to Oligocene age is found in isolated on-shore outcrops and in the subsurface of the Suez Gulf. Typical deposits include sandstone units in fault-bound basins, displaying an upward transition into evaporitic beds. In this synrift sequence, faults have been recorded in the Nukhul Formation, which is dominated by shallow-marine, fine- to medium-grained sandstone. This unit is poorly to moderately consolidated and is assumed to have been located within some hundred meters from the surface during the onset of rifting.

To illustrate the common characteristics of extensional faults in siliciclastic rocks, the description starts with two case studies; the Baba village and Tayiba mine faults (Figure 6, marks 1 and 2, respectively). The case studies set the standard for the following quantitative analysis of 26 fault cores. Both case studies are based on outcrops in the Nubian Sandstone.

Baba Village Fault

In the studied cliff-section exposure, the Baba village fault has a throw of approximately 12 m (39 ft) (Figure 7). This fault juxtaposes a footwall section of meter-thick sandstone beds separated by thin mudstone layers, with a hanging-wall section of mainly thin-bedded sandstone. Both units belong to the Cambrian Abu Thora Formation of the Ataqua Group. Toward the core, layering shows a slight drag on the footwall side. In the hanging wall, a rollover higher in the section replaced by a drag fold farther down is observed. In more detail, a complex zone of concentrated shear, the fault core, can be distinguished because of its pervasive deformation and the fact that layers across the core zone are nonjuxtaposed. The surrounding damage zone shows deformation bands and some slipped deformation bands (Rotevatn et al., 2008) in sand layers and fractures in mudstone, of which many show centimeter- to decimeter-scale displacement. The intensity of deformation appears to be highest in the inner footwall damage zone and in the rollover hinge of the hanging wall. Internally, the core consists of one principal slip surface toward the hanging wall, additional subordinate slip surfaces toward the footwall, and semicontinuous layer(s) of gouge from brittle deformation of shale (shale

Figure 5. Facies classification scheme of fault lenses (L) in sandstone-shale units. The type facies relates to the lithology and degree of internal deformation. Shapes are defined by the bounding margins (slip surface or membrane) and their orientation in a Riedel system. See the text for further description.

gouge) and gouge from cataclasis of sand (sand gouge). These two elements bound lenses consisting of both sandstone and sandstone-mudstone, which have moved along the fault and thus are not juxtaposed to the beds they originated from.

Tayiba Mines Fault

This fault has a throw of 100 m (328 ft) in the study area, juxtaposing the lower and upper parts of the Jurassic–Lower Cretaceous Malha Formation. This fault cuts thick-bedded fluvial and fluvially reworked eolian sandstones with some thin gravel and mudstone layers, overlying a thick claystone unit exposed in the footwall. Figure 8 shows a vertical section of the fault core in a quarry, which allows a 3-D analysis of the fault core and footwall in a 60 m (197 ft) (length) × 50 m (164 ft) (width) × 6 m (20 ft) (height) rock volume. Similar to the

Baba village fault, this fault is complex with several structural elements, including (1) fault-rock layers as fault-parallel membranes, (2) lenses of various composition, (3) slip surfaces and fractures, and (4) deformation bands, of which some are fractured. The principal slip surface of the core sits toward the hanging wall, whereas associated slip surfaces appear in an open network that can be traced along fault strike through the study area. Bounding membranes consist of sand gouge, shale gouge, mixed shale gouge with sand grains, and claystone-derived breccia. Membranes are up to 10 cm (4 in.) thick with a substantial spatial extent but are not continuous laterally. Fault-rock membranes and slip surfaces bound lenses of sandstone and shale. Sandstone lenses are in general less than 10 cm (4 in.) thick and several meters long and exhibit internal deformation-band networks. Shale lenses show similar internal networks but exhibit shear fractures
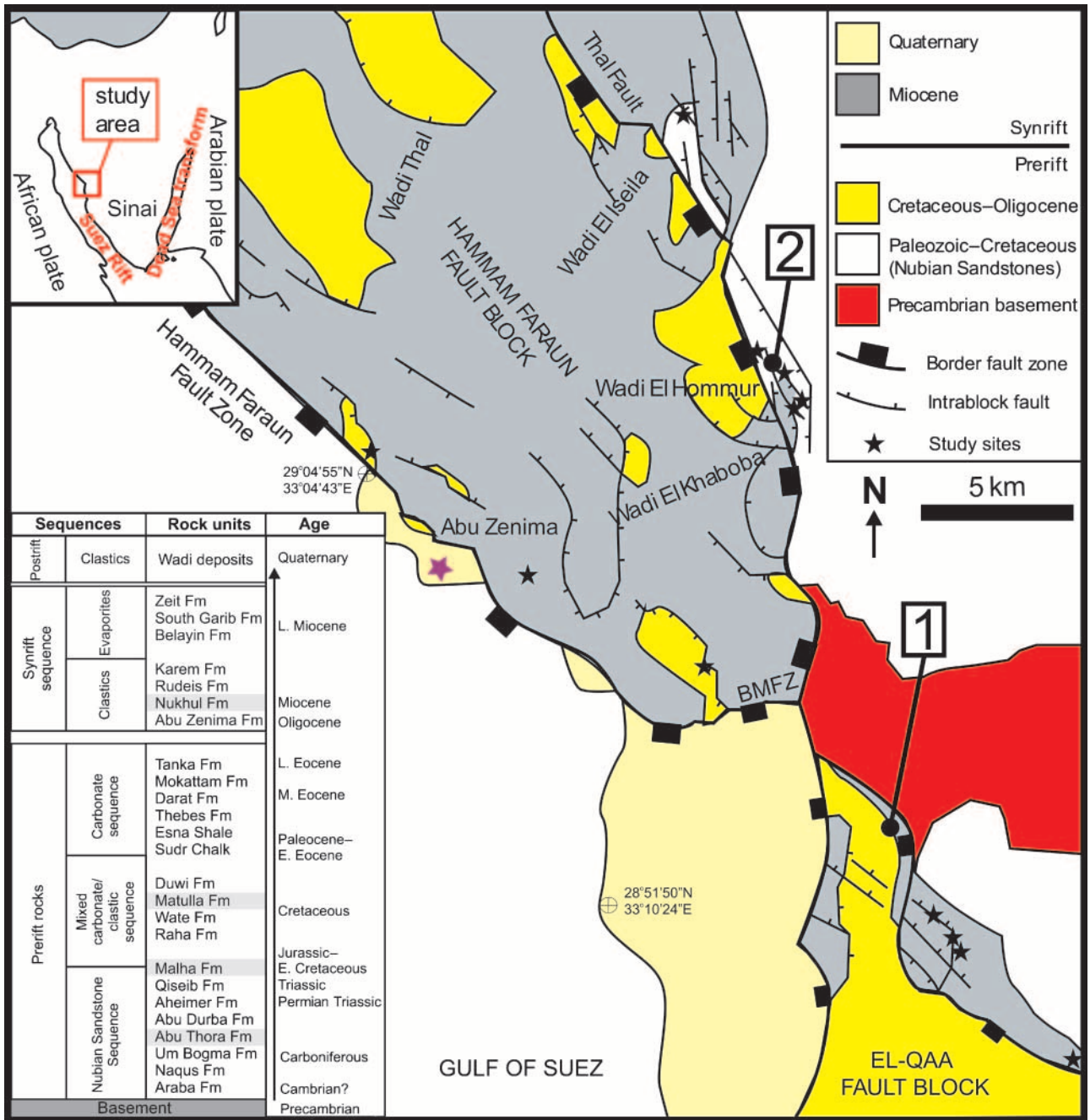
Figure 6. Geological map of western Sinai showing the main lithological units and major faults. Stars indicate the sites that host the studied faults. See Table 1 for detailed locations (coordinates). The Baba village fault is labeled 1, and the Tayiba mines fault is labeled 2. The stratigraphic column shows rock sequences, units, and their age (modified from Moustafa, 2004). The four units with underlying shading are the formations in which faults have been studied. BMFZ = Baba Markha fault zone.

instead of deformation bands. The damage zone reveals deformation bands in sandstone and fractures in mudstone. The damage zone can be mapped 15–25 m (49–82 ft) into the footwall, whereas the width of the hanging-wall damage zone is uncertain because of interference with a neighboring fault.

General Characteristics of Fault Database

Several variables related to the 26 studied fault outcrops differ from data set to data set. Despite this, the fault-facies analysis reveals common elements that can be compared and analyzed. Most

Table 1. Summary of Fault Data as Recorded on Various Sites*

Case	Location	Unit	Lithification	Throw (m)	Burial (m)	Juxtaposition	Window	Thick. (Max-Min)
Tayiba mines	N29°06.7-33°14.3	Thick-bedded medium-course sandstone with thin mud layers	Mod.	100	<1500	Self	6/100	0.68–0.73
Tayiba mines	N29°06.7-33°14.3	As above	Mod.	100	<1500	Self	As above	0.25–0.35
Tayiba mines	N29°06.7-33°14.3	As above	Mod.	100	<1500	Self	As above	0.20–1.50
Wadi Baba	N28°55.5-33°18.2	As above	Mod.	100	<1500	Self	5/100	0.8–0.21
Wadi Baba	N28°55.5-33°18.7	As above	Mod.	100	<1500	Self	8/100	0.12–0.18
Wadi Baba	N28°55.5-33°18.7	As above	Mod.	2.35	<1500	Self	2.20/2.35	0.004–0.037
Wadi Iseila	N29°12.1-33°12.1	As above	Mod.	20	<1500	Self	8/20	0.08–0.30
Wadi Baba	N28°55.6-33°18.2	HW = thick-bedded medium-course sandstone with thin mud layers; FW = moderately bedded sandstone + shale	Mod.	200	<1500	Non	22/200	1.0–1.5
Wadi Baba	N28°55.6-33°18.2	As above	Mod.	200	<1500	Self	10/200	1.0–1.3
Wadi Baba	N28°55.6-33°18.2	As above	Mod.	200	<1500	Self	10/200	0.2–0.3
Wadi Baba	N28°55.6-33°18.2	As above	Mod.	7	<1500	Self	1/7	0.2–0.25
Baba village	N28°57.3-33°17.2	Thick-bedded sandstone + layers of shale	Mod.	12	<2000	Self	2/12	0.053–0.15
Thal fault	N29°10.2-33°12.5	FW = fine–medium sandstone; HW = synrift fine sand	Mod.	943	<1800	Non	3/943	0.9–1.0
Thal fault	N29°07.5-33°13.4	FW = thick-bedded sandstone + shale; HW = limestone + synrift fine sandstone	Mod.	1312	<1500	Non	20/1312	0.9–1.2
Sidri fault	N28°52.6-33°21.7	FW = fine–medium sandstone and shale layers; HW = synrift fine sandstone	Mod.	2000	<2000	Non	15/2000	0.14–21
Nukhul Basin	N29°01.2-33°12.3	FW = gravel bed and fine sandstone; HW = thin-bedded mudstone	Low	12	<200	Self	4/12	0.29–0.40
Nukhul Basin	N29°01.2-33°12.3	As above	Low	12	<200	Non	4/12	0.05–0.08
Nukhul Basin	N29°01.2-33°12.3	As above	Low	12	<200	Non	4/12	0.018–0.12
Wadi Kaboba	N29°06.2-33°13.6	Synrift thick-bedded fine sandstone	Poor	20	<200	Self	7/20	0.15–0.6
Wadi Kaboba	N29°06.2-33°13.6	As above	Poor	15	<200	Self	4/20	0.25–1.2
Abu Zenima	N29°04.3-33°05.6	Synrift thick-bedded massive fine sandstone	Poor	3	<200	Self	3/3	0.02–0.1
Abu Zenima	N29°04.3-33°05.6	As above; with a thick shale layer	Poor	7	<200	Non	5/7	0.1–0.8
Abu Zenima	N29°05.1-33°04.7	As above	Poor	0.5	<200	Self	2/0.5	0.02–0.05
Wadi Kaboba	N29°06.2-33°14.6	Thick-bedded medium-course sandstone, thin mud layers	Mod.	6.2	<1500	Self	6/6	0.028–0.35
Wadi Baba	N28°55.2-33°18.1	FW = thick-bedded medium sandstone; FW = thin-bedded shale + sandstone	Mod.	30	<1500	Non	5/30	0.3–0.5
Wadi Matulla	N29°02.8-33°08.3	Thick-bedded fine-medium sandstone and thin shale layers	Mod.	7	<800	Self	5/7	0.1–0.6

*The database covers the location, general fault characteristics, discrete structures, membranes, and lenses. For fault-facies classes, see Figures 3–5. The data sets are analyzed in Figures 9–14. DS = discrete structure; HW = hanging wall; FW = footwall; INT = internal; C = continuous; S = semicontinuous; I = isolated; Ssl = slip-surface type; Ss = slip-surface shape; Sdb = deformation band type; Sfr = fracture; Mt = membrane type; Mf = membrane fault rock; Mc = membrane cement; Lt = lense type; Ls = lense shape; Mod. = moderate.

Discrete Structure Type	Slip-Surface Position	DS Continuity	DS-Type Facies	DS-Shape Facies	Membrane-Type Facies	Membrane-Shape Facies	Lens-Type Facies	Lens-Shape Facies
Ssl, Sfr, Sdb	HW	C, S, 2*I	2*Ssl3, Sdb1, Sdb4	Ss3-C, Ss5-C, 2*Ss5	Mt2, Mt2-C, Mt3	2*Mf1, Mc1	LtA5	Ls4
Ssl, Sfr, Sdb	HW	C, S, I	Ssl3, Ssf1, Ssf4, Sdb1, Sdb3	Ss3-C, Ss5-C, Ss4-B	Mt1, Mt2, Mt2-C, Mt3	2*Mf1, Mf3, Mc1	LtA4, LtA5, LtB3	3*Ls4
Ssl, Sfr, Sdb	HW	C, 2*I	Ssl3, Ssf1, Ssf4, Sdb1, Sdb4	Ss3-C, Ss5-C, Ss4-B, Ss5-B	Mt1, Mt2, Mt2-C, Mt3	Mf4, Mf3, Mc2, Mf2	LtA3, LtA4	Ls4
Ssl, Sfr	HW, INT	2*C	Ssl3, Sfr1, Sfr3	Ss3-C, Ss1-C	Mt2, Mt2-C, Mt3	2*Mf1, Mc1	LtD-1	Ls4
Ssl	INT	C	Ssl3	Ss1-C	Mt2, Mt2-C, Mt3	Mf1, Mc2, Mf2		
Ssl	HW, INT	C	Ssl3	Ss1-C	Mt2	Mf3		
Ssl, Sfr, Sdb	HW, FW	C, 2*S	2*Ssl3, Ssl1, Ssl4, Sdb1, Sdb4	Ss1-C, Ss3-C, Ss4-C, Ss3-B, Ss4-B	Mt2	Mf2, Mf3	LtA3, LtA4, LtD-1, 5*LtD-2	Ls3, 6*Ls4, Ls5
Ssl, Sdb	HW, FW	C, I	Ssl3, Sdb1	Ss1-C, Ss3-B	Mt3	Mf1	2*LtA3, LtC4	Ls3, 2*Ls4
Ssl	HW, FW	C	Ssl1, Ssl3	Ss3-C	Mt1, Mt3	2*Mf1	LtC3	Ls4
Ssl, Sfr	HW	C, I	Ssl1, Sfr3	Ss1-C, Ss4-C	Mt2, Mt3	2*Mf1	LtA3	Ls4
Ssl	HW	C	Ssl3	Ss1-C	Mt3, Mt3-C	Mf1, Mc1	LtA2	Ls4
Ssl	HW	C	Ssl3	Ss3-C	Mt1, Mt3	Mf4, Mf2	LtC1, LtC2, 3*LtC3	2*Ls3, 3*Ls4
Ssl, Sfr	HW, FW	C, S	Ssl3, Sfr1	Ss3-C, Ss6-C	2*Mt1, Mt2, Mt4	4*Mf1		
Ssl	HW	C	Ssl3	Ss3-C	Mt1, Mt3	2*Mf1	LtA3	Ls4
Ssl	HW	C	Ssl3	Ss3-C	Mt1-C, Mt1, Mt2, Mt3	2*Mf1, Mc4, Mf3	LtC3, LtB3, LtA3	4*Ls4
Ssl	FW	C	Ssl3	Ss3-C	Mt1, Mt1-C, Mt4	2*Mf3, Mc4	LtA3, LtB2	Ls4, Ls4
Ssl	HW	C	Ssl3	Ss3-C	Mt1	Mf1		
Ssl	HW	C	Ssl3	Ss3-C	2*Mt3	Mf1, Mf2	LtC4	Ls4
Ssl Sfr	HW, FW	C, I	Ssl3 Sfr1	Ss3-C, Ss4-C	Mt1-C, Mt2, Mt3	Mc4, Mf2, Mf5	LtA2, LtA4, 5*LtA3	2*Ls3, 4*Ls4, Ls5
Ssl, Sdb	HW	C, I	Ssl3, Sdb1	Ss1-C, Ss3-B	Mt1-C, Mt2	Mc5, Mf1	2*LtA3	2*Ls4
Ssl, Sfr	HW	C, I	Ssl3, Sfr1	Ss1-C, Ss4-C	Mt1-C, Mt2, Mt3	Mf2, Mf4, Mf5		
Ssl	HW	C	Ssl3	Ss1-C	Mt1, Mt3	Mf3, Mf4	LtB2	Ls4
Ssl	HW	C	Ssl3	Ss1-C	Mt1	Mf1		
Ssl		2*S	Ssl1, Ssl3	Ss3-C, Ss3-C	Mt2, Mt2-C	Mf1, Mc3	2*LtA4	2*Ls4
2*Ssl	HW, FW	2*C	2*Ssl3	Ss1-C, Ss1-C	Mt1, Mt2, Mt3	Mf3, 2*Mf4	3*LtA3	3*Ls4
Ssl	HW	C	Ssl3	Ss1-C	Mt3	Mf1	2*LtB2	2*Ls3

of the faults are from the Nubian Sandstone Group, with additional faults from the Matulla and Nukhul formations (Figure 6, Table 1).

The data sets presented here are based on the 2-D view generally allowed by outcrop observations, as exemplified by Figures 7 and 8. Data were collected at each fault outcrop by carefully mapping individual structural elements of the core. The maps were subsequently analyzed for position and length of discrete structures, membranes and lenses, and cement if this element was present as distinct layers or pockets. For elements of spatial significance (membranes and lenses), the length of the element along the fault, the C axis, and the maximum width of the element normal to the fault, the A axis, were measured. In some cases, and especially for membranes, elements were traced to the end of the exposure, thereby giving minimum length numbers. In the facies analysis, all individual elements were classified according to facies classes (Figures 3–5).

In Figure 9, the general characteristics of the studied faults are summarized. A minority of the faults have displacements that exceed the formation thickness, and the formation is thereby nonjuxtaposed (Figure 9A). For large-displacement faults, a significant stratigraphic section has passed any given point in the fault core, whereas for small-displacement faults, a small section can be represented in the fault core. The throw of the 26 faults varies significantly; from less than 1 m (3 ft) to nearly 2000 m (6562 ft); most of the faults exhibit throws between several meters and 100 m (328 ft) (Figure 9B). Most of the faults in the database juxtapose thick (>10 m [33 ft]) sandstone units with moderately (2–10 m [6–33 ft]) layered sandstones, which were moderately (Nubian Sandstone and Matulla formations) to poorly consolidated (Nukhul Formation) at the time of deformation. Most of the fault cores are complex in that they are made up of combinations of slip-surface, membrane, and lens elements (LMS, Figure 9F). More simple cores exhibit slip surface(s) and membrane(s) as constituents. A comparison of the areal distribution of fault-core elements with respect to surface area shows no clear pattern (Figure 9G).

Outcrop-based studies of faults are challenging because only a part of the structure of interest can be observed. In extensional faults, this uncertainty can be estimated by comparing the throw of the fault with the height of the exposure. The throw versus height of the exposure data can be fitted by a power regression trend with an exponent (n) lower than 1.0 (diamonds in Figure 10). This indicates that the height of the exposure represents a progressively smaller window of the fault as fault throw increases. Therefore, this trend expresses the larger uncertainty with increased throw. This uncertainty can also be described by a so-called window of observation, which is equal to the height of the exposure divided by the fault throw. The window of observation decreases from 10 times the fault throw for faults of less than 1-m (3-ft) throw to less than 0.1 times the fault throw for faults with throw greater than 100 m (328 ft) (squares in Figure 10).

Analysis of the data on fault-core width shows that throw versus thickness of the fault core for the 26 faults can be fitted either by a linear or power regression line (Figure 11A). The thickness of the core varies significantly even for individual sites (Figure 11B). Despite this fact, when throw is compared with the average fault-core thickness, the plot reveals a possible power trend line. Fault-core thickness in a 2-D view depends basically on the spatial extent of two elements: membranes and lenses. However, in our data, poor correlation between fault-core thickness and the proportion of lenses versus membranes is observed (Figure 11C).

Discrete Structures

Slip surfaces are key elements for throw accumulation in fault cores. In the analyzed data set, they are in most cases located toward the hanging wall, as shown in Figure 12A, implicitly supporting the theory that elements in the fault core commonly come from the footwall (e.g., Davatzes and Aydin, 2003). In the outcrops studied, slip surfaces appear to be continuous; however, this may be only the case in the limited 2-D window of observation. Principal slip surfaces and most subordinate slip surfaces are subparallel to the overall fault core
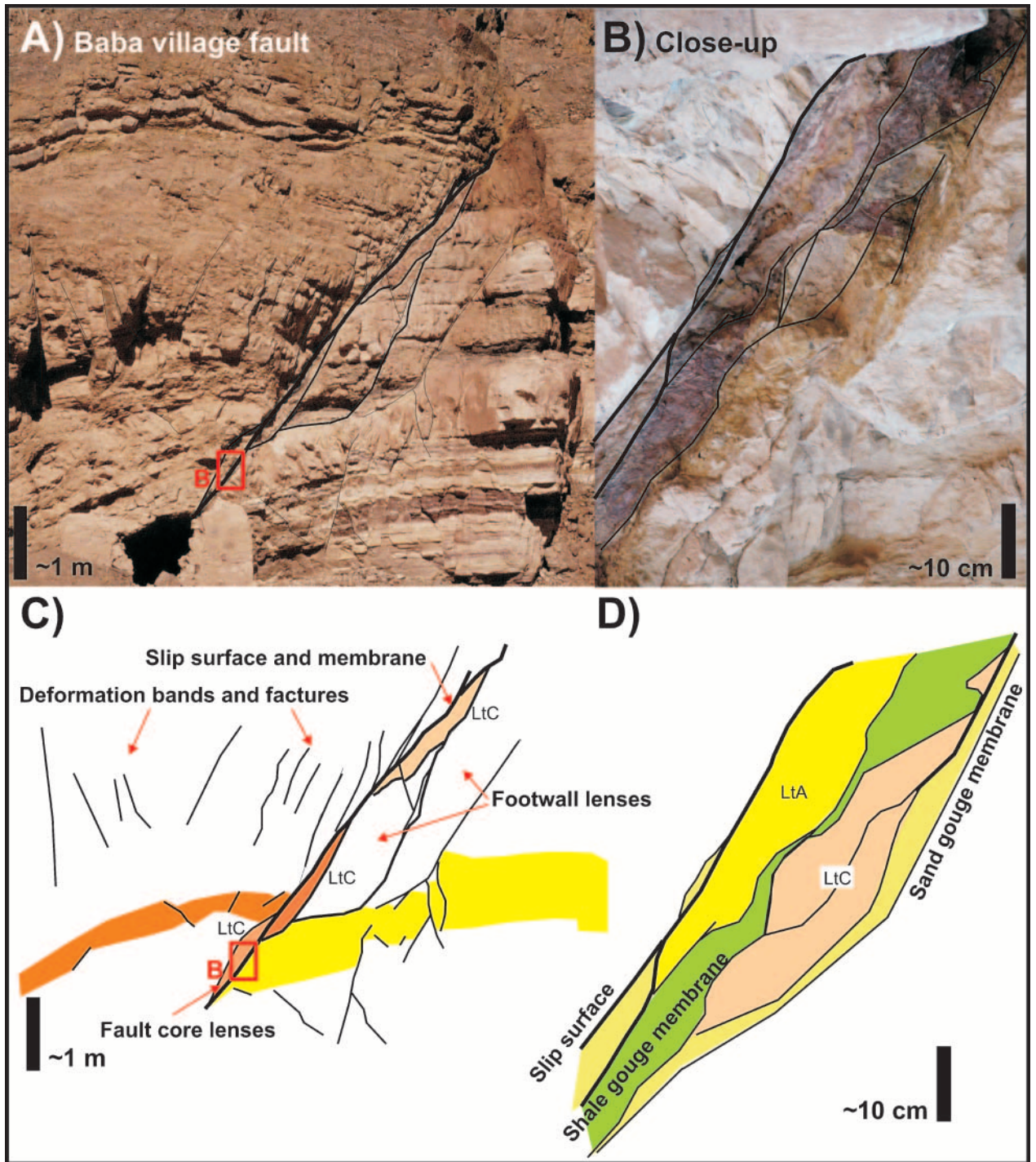
Figure 7. (A) Photograph of the Baba village fault located in the footwall of the major Baba fault (Sharp et al., 2000); see Figure 6 for the location. The fault juxtaposes sandstone units of the fluvial Cambrian Ataqua Group (lowermost Nubian Sandstone unit) and has an estimated throw of 12 m (40 ft). Lines outline key structures. (B) Close-up photograph of a part of the fault (red box in A), showing the details of the narrow zone of concentrated shear, the fault core. Note the position of the slip surface, the red mudstone with clasts of sandstone as a layer along the core, and the highly deformed sandstone hosting some cement as a tan layer along the core to the right. These fault-parallel layers, locally in concert with a slip surface, bound lenses within the core. (C) Interpretation of the 2-D fault view presented in panel A, with marker beds highlighted for illustration purposes. Note the long, thin lenses of the fault core. (D) Interpretation of the close-up photograph of panel B, showing fault-parallel layers (membranes) of shale gouge and sand gouge, slip-surface(s), and lenses. Code used on lenses: LtA = lens type that consists of sandstone; LtC = lens type that consists of sandstone and mudstone layers (see Figure 5 for classification).

Figure 8. (A) Photograph of the quarry wall in the Tayiba mine found in the footwall of the major Thal fault (Sharp et al., 2000; Moustafa, 2004); see Figure 6 for the location. The Tayiba mine fault has a throw of 100 m (328 ft), with footwall and hanging-wall sandstones belonging to the mainly fluvial Jurassic–Cretaceous Malha Formation. (B) Interpretation of the 2-D fault view, showing a principal slip surface, sandstone and sandstone-claystone lenses, and several types of fault-rock layers parallel to the fault.
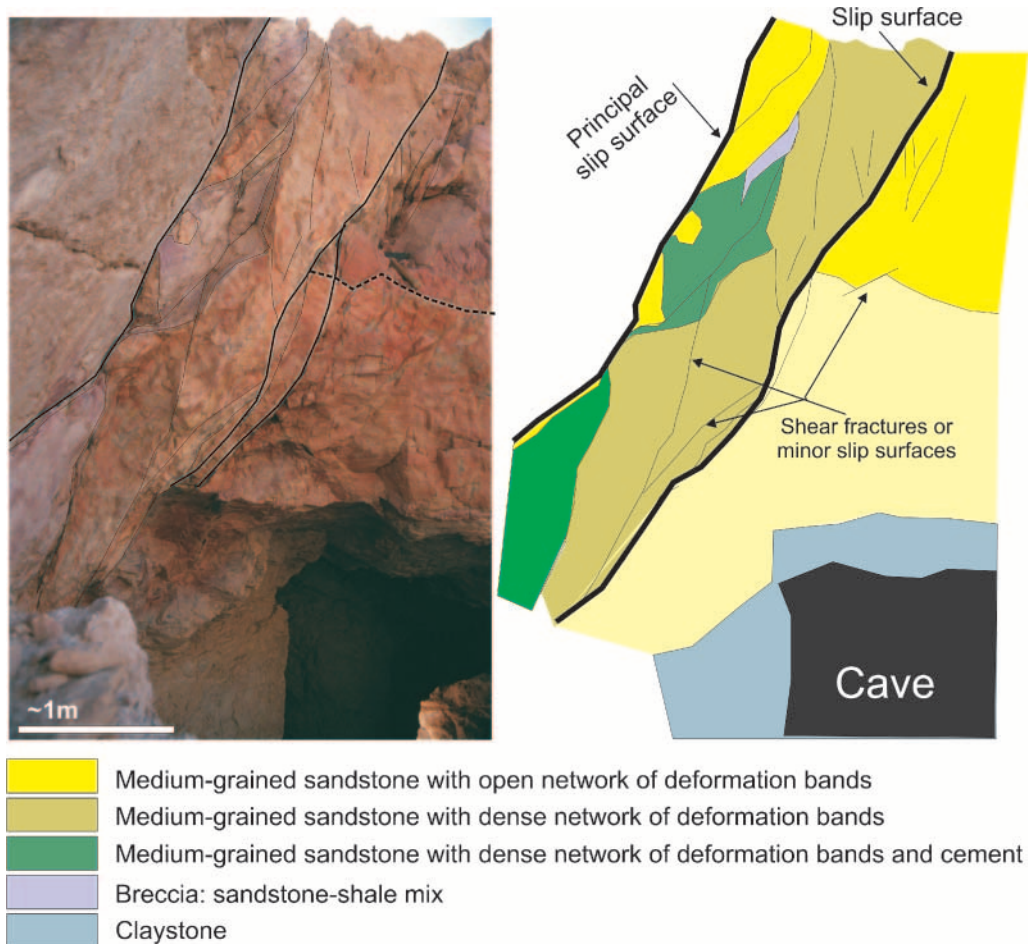
(Y orientation), but some P and R orientations are observed for minor slip surfaces that form open networks (Figure 12A–D).

Analysis of sandstone lenses in the core shows a dominance of mostly shear-related deformation bands, as expressed in Figure 12E and F. Such bands are mostly made up of R orientations, but P and Y orientations also exist. Most bands occur in dense to open networks. Similarly, fractures in shale lenses tend to be shear related with R, Y, and P orientations in decreasing numbers. Most fractures are found in dense to anastomosing networks (Figure 12D, H).

Membranes

In 2-D outcrops, membranes found in an extensional fault can be described by their length along the layer versus maximum thickness, the C versus A axis, respectively. In the analyzed data set (Figure 13), the membranes are very long as compared to thickness, with an average C/A ratio of approximately 100. However, for these data, an upper cutoff for the C-axis is observed because membranes in many cases are longer than the exposure (11 of 46 data points). Most observed membranes consist of sand and shale gouge or breccia, with a few cases of sand smear. Shale smear is not observed in the studied sand-dominated lithologies. The shape of the membranes is mostly continuous through the outcrop, with fewer semicontinuous to ruptured and patchy membranes. Very few membranes have pocket shape.

Of the total data set on membranes, 12 of 61 data points (about 20%) represent distinct occurrences of oxide cement in the faults. A common observation is that cement appears as more or less continuous layers along boundaries characterized
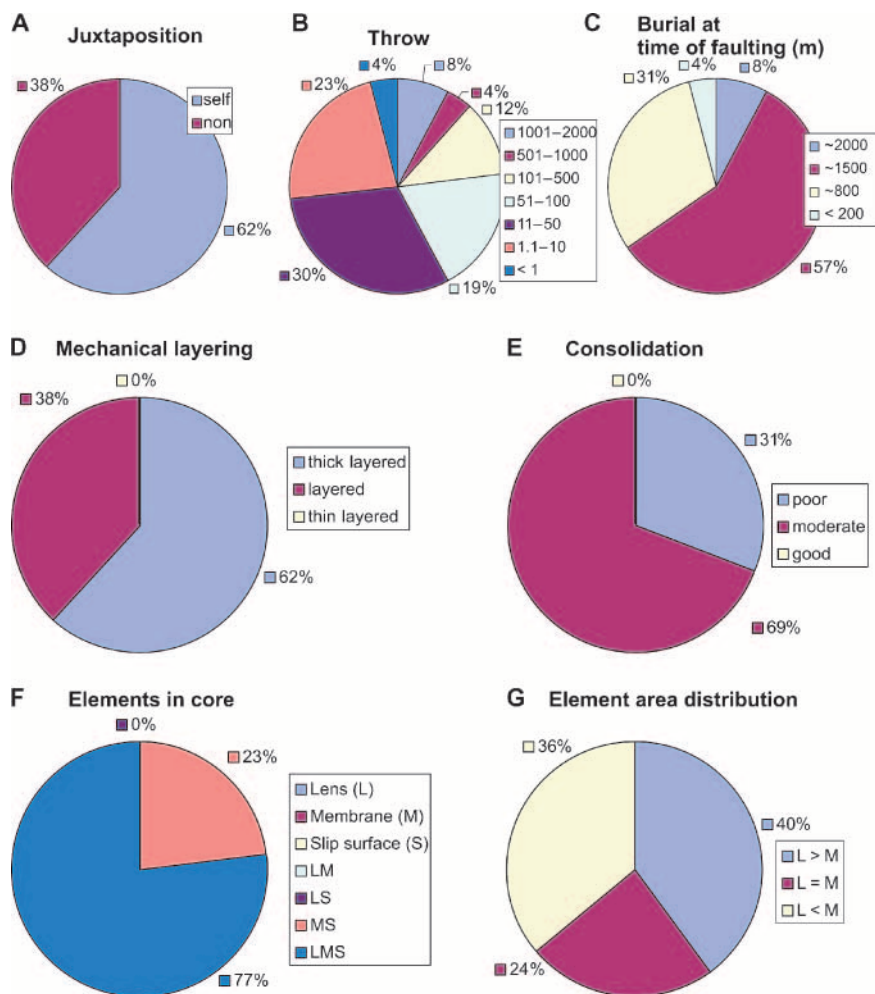
Figure 9. Basic information for the analyzed 26 faults, all presented as percentages. All faults are extensional, showing sandstone-sandstone juxtaposition. (A) Nonjuxtaposed faults placing the footwall formation in contact with a different formation in the hanging wall versus faults that juxtapose the same formation in the footwall and hanging wall. (B) Throw (vertical separation) on faults, categorized according to ranges (0–1 m, 1–10 m [0–3 ft, 3–33 ft], etc.). (C) Predicted burial at the onset of faulting, categorized according to ranges (0–200 m, 200–800 m [0–656 ft, 656–2625 ft], etc.). (D) Effect of layering as an indicator for mechanical behavior during deformation, as predicted from layer thickness and the distribution of sandstone and shale units. Note that Sinai is dominated by thick sandstone sections. (E) Assumed degree of lithification. (F) Observed lenses, membranes, and slip surfaces in the fault core; LM = lens and membrane; LS = lens and slip surface; MS = membrane and slip surface; LMS = lens, membrane, and slip surface. (G) Spatial extent of lenses (L) and membranes (M).

by change in grain size, possibly reflecting transitions in permeability. For instance, cement is frequently found in well-preserved sandstone next to a deformation-band swarm or slip zone. Some fault-core lenses also host extensive cement, in such cases revealing a dense network of deformation bands (Figure 8). Breccias are also locally cemented. In this analysis, cement is included in the membrane appearance classes. The data show a tendency for continuous shapes, but with all shapes significantly represented (Figure 13D).

Lenses

As for membranes, lenses of extensional fault cores can be described by their length versus thickness ratio (C and A axes). The data show that most lenses

have a C axis in the range of decimeter to meter scale, with a C/A ratio ranging from 5 to 20 and an average C/A ratio of approximately 9 (Figure 14A). Commonly, the lenses contain an open network of discrete structures (Lt3), but dense networks to isolated structures are also observed (Lt4 and Lt2 of Figure 5). Analysis of lens shapes reveals a clear tendency for four-sided lenses (Ls4), but the data set also shows significant numbers of three-sided and five-sided lenses (Ls3 and Ls5, Figure 14B, C). When analyzing sandstone lenses separately, the common observations for all lenses, as discussed above, are repeated. A minor difference in the sandstone lenses is a stronger tendency for open and dense networks of discrete structures, in this case, deformation bands (LtA3 and LtA4, Figure 14D, E).
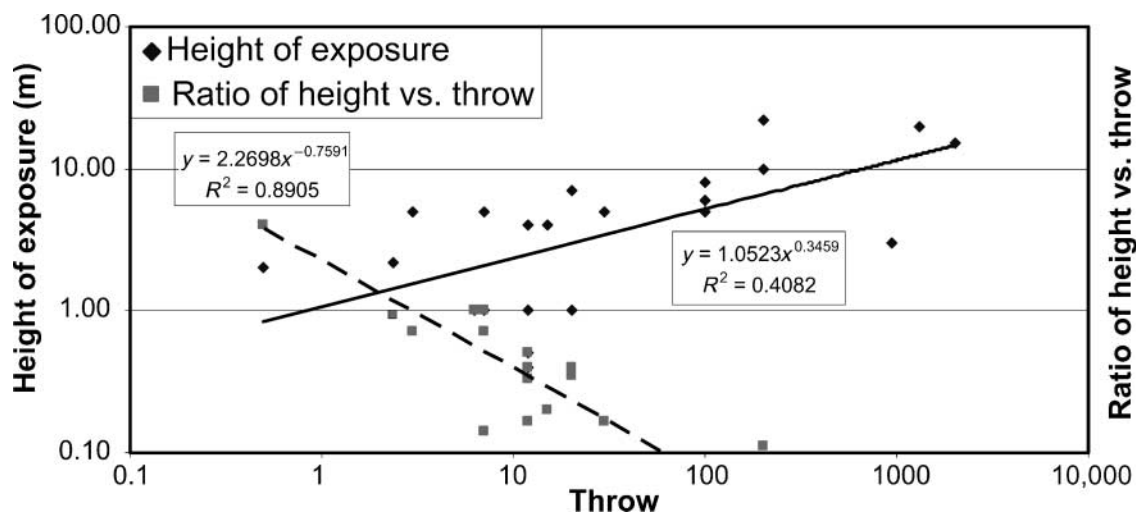
Figure 10. Plot showing the throw of studied faults versus the height of the mapped exposure, and the throw versus height of fault exposure divided by throw. Both sets of data points reveal a power-law trend and a reduction of the window of observation with fault throw.

DISCUSSION

Traditional facies analysis of sedimentary rocks helps the observer to identify features or rock bodies with similar characteristics. Identifying patterns of facies distributions provides a powerful tool for forecasting property distributions in the subsurface. The fault-facies approach applies this methodology to fault-related features. Identifying fault facies within a fault envelope allows the identification of bodies, the fundamental building objects in volumetric descriptions. In this context, the term fault architecture becomes meaningful, in that the facies descriptions and pattern analyses are used in fault model building (see discussion by Peacock, 2008; Wilson, 2008). Thereby, architecture describes the design of the fault with elements that have distinct compositions, shapes, and positions in the fault envelope.

Any fault facies will have a set of common characteristics (i.e., geometry, dimensions, and petrophysical properties) that can be quantified depending on the scale and level of detail required to meet the objectives of the study. At present, examples of quantification of fault features include, among others, scaling laws on fault-core thickness versus fault throw in siliciclastic sedimentary rocks (e.g., Childs et al., 1996; Sperrevik et al., 2002; Shipton et al., 2006), the relationship

between fault throw and the width of damage zones in sandstone (e.g., Beach et al., 1999; Shipton and Cowie, 2001; Schueller et al., 2007), and the scaling laws established for deformation bands and fractures in both sedimentary and crystalline rocks (e.g., Barton, 1995; Vermilye and Scholz, 1995; Marrett, 1996; Odling, 1997). Furthermore, Schultz et al. (2008) documented that a dependence of displacement-length scaling for fractures and deformation bands exists. However, much remains to be established on a more detailed level, for example, the structural element distribution in marginal parts of fault-strain envelopes, the shape and size of lenses, the general distribution and shape of fault-rock membranes, and the impact of diagenesis. The shape of fault-rock membranes has been addressed in several studies of shale gouge ratio, shale smear factor (SSF), and clay smear ratio (Lindsay et al., 1993; Yielding et al., 1997), which are used to estimate transmissibility multipliers for flow across faults (Walsh et al., 1998; Manzocchi et al., 1999). These 3-D techniques are well established and work well with faults displaying single discrete planes. However, because these methods essentially integrate all effects caused by fault components and geometry into a function of shale gouge, clay smear, and juxtaposition, thereby obscuring the presence and effects of fault element distribution and properties, they are not directly applicable
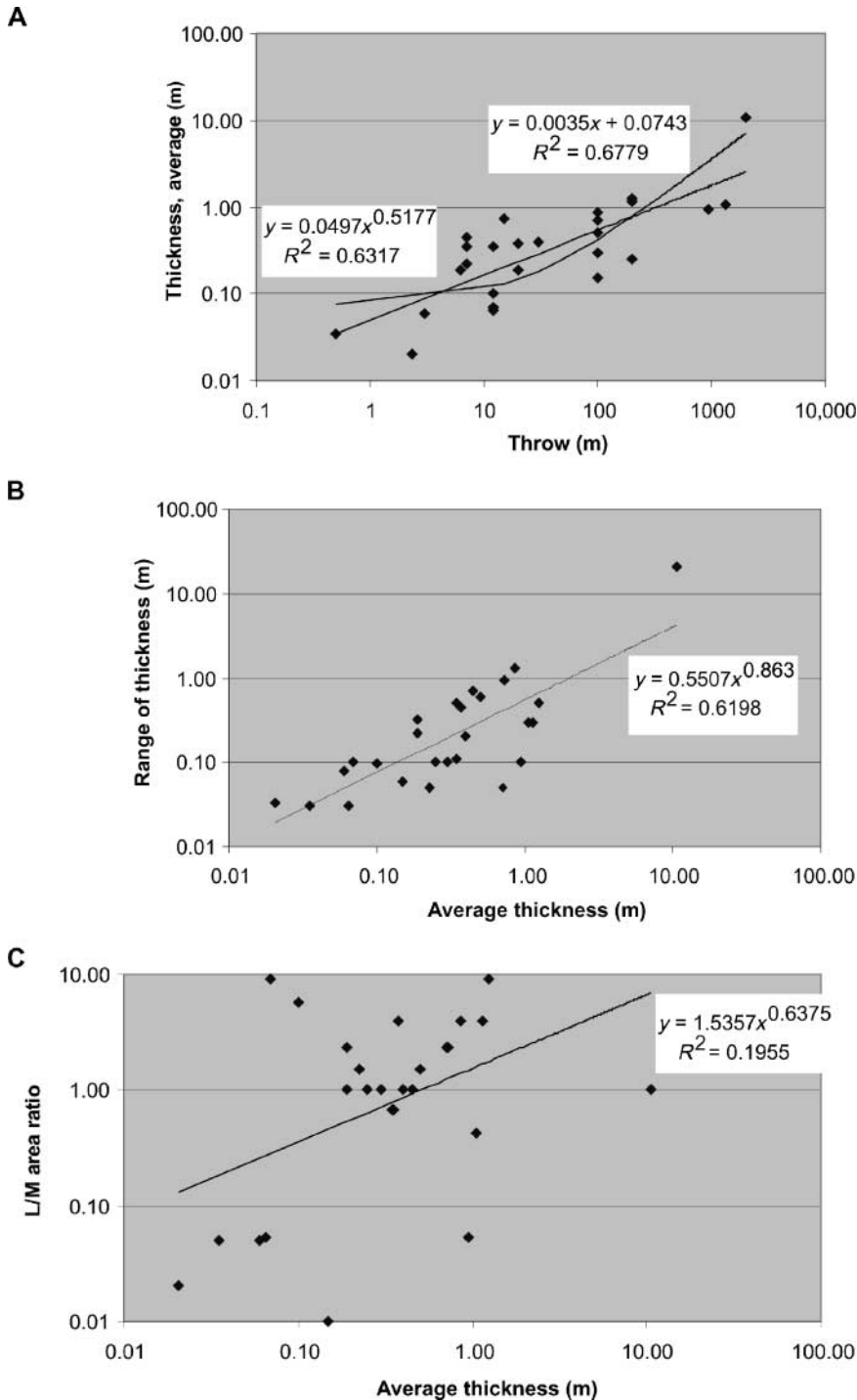
Figure 11. Data from the 26 faults analyzed. (A) Throw versus average thickness of the fault cores. A power-law or linear regression line fits the data. Note that the power law has $n = 0.52$, which seems to be a general number encountered for fault thickness. (B) Average thickness versus range of thickness (maximum minus mini>mum) for studied faults. A power-law regression line fits the data. (C) Average thickness versus ratio between predicted spatial extents of lenses (L) divided by spatial extents of membranes (M). The data set shows no statistical trend.

in fault-facies analysis. They only average out parts of the fault envelope.

The new approach to fault description represented by facies analysis of 26 fault outcrops from Sinai (Egypt) could be considered a first step toward a global fault-core database. Despite the moderate number of observations, the analysis renders valuable information on extensional fault cores in siliciclastic units. The average width of the core relates to throw on the fault, consistent with a linear or power-law trend line (Figure 11), which is in agreement with several studies on fault-core thickness (Walsh et al., 1998; Fossen and Hesthammer, 2000; Sperrevik et al., 2002; Shipton
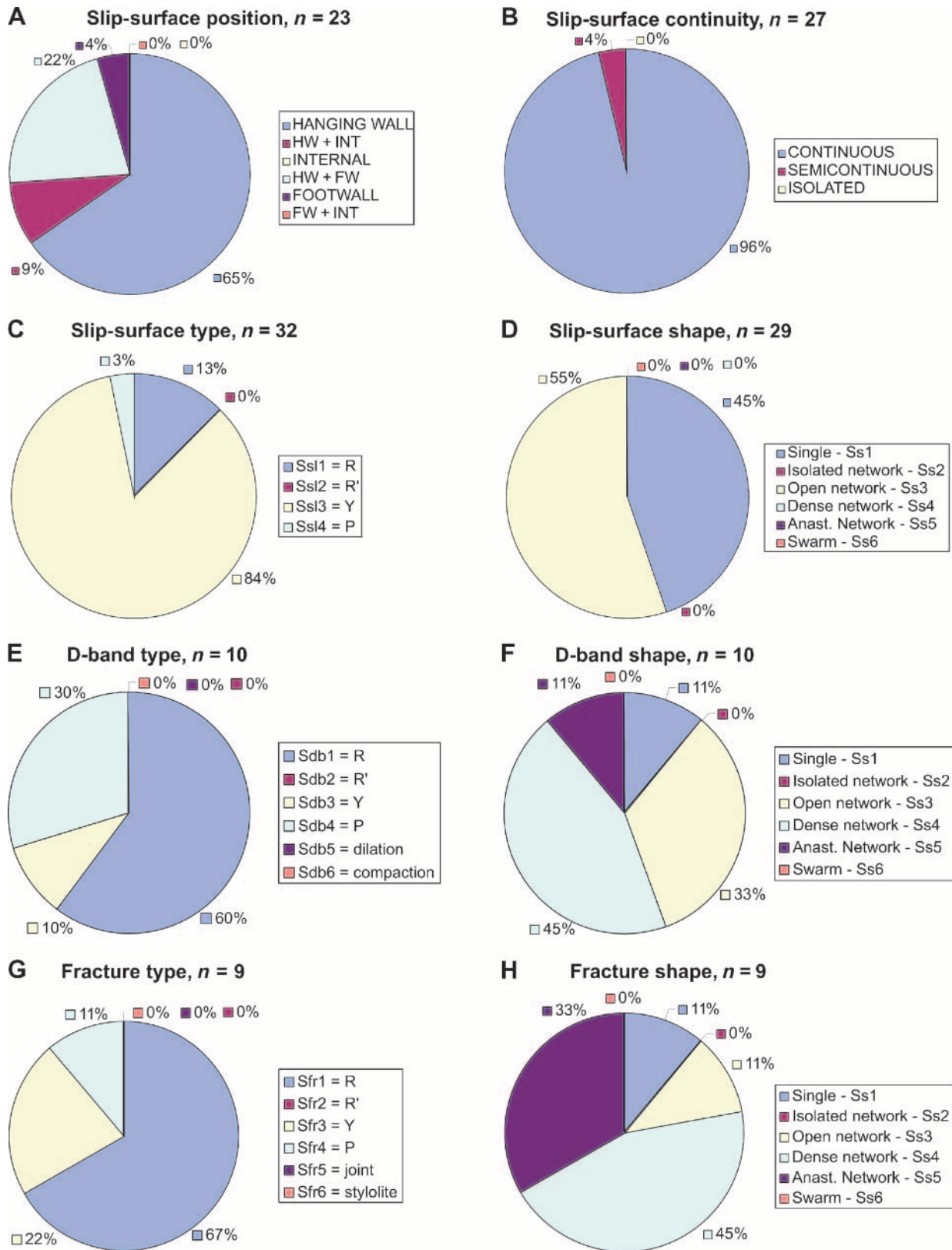
Figure 12. Results from analysis of discrete structures, shown as percentage of the data set. The classifications used are presented in Figure 5. (A) Position of slip surfaces in the fault core (HW = hanging-wall side; FW = footwall side; INT = internal to the core); (B) continuity of slip surfaces; (C) type of slip surfaces; (D) shape of slip surfaces; (E) type of deformation bands (D bands); (F) shape of deformation bands; (G) type of fractures; (H) shape of fractures.
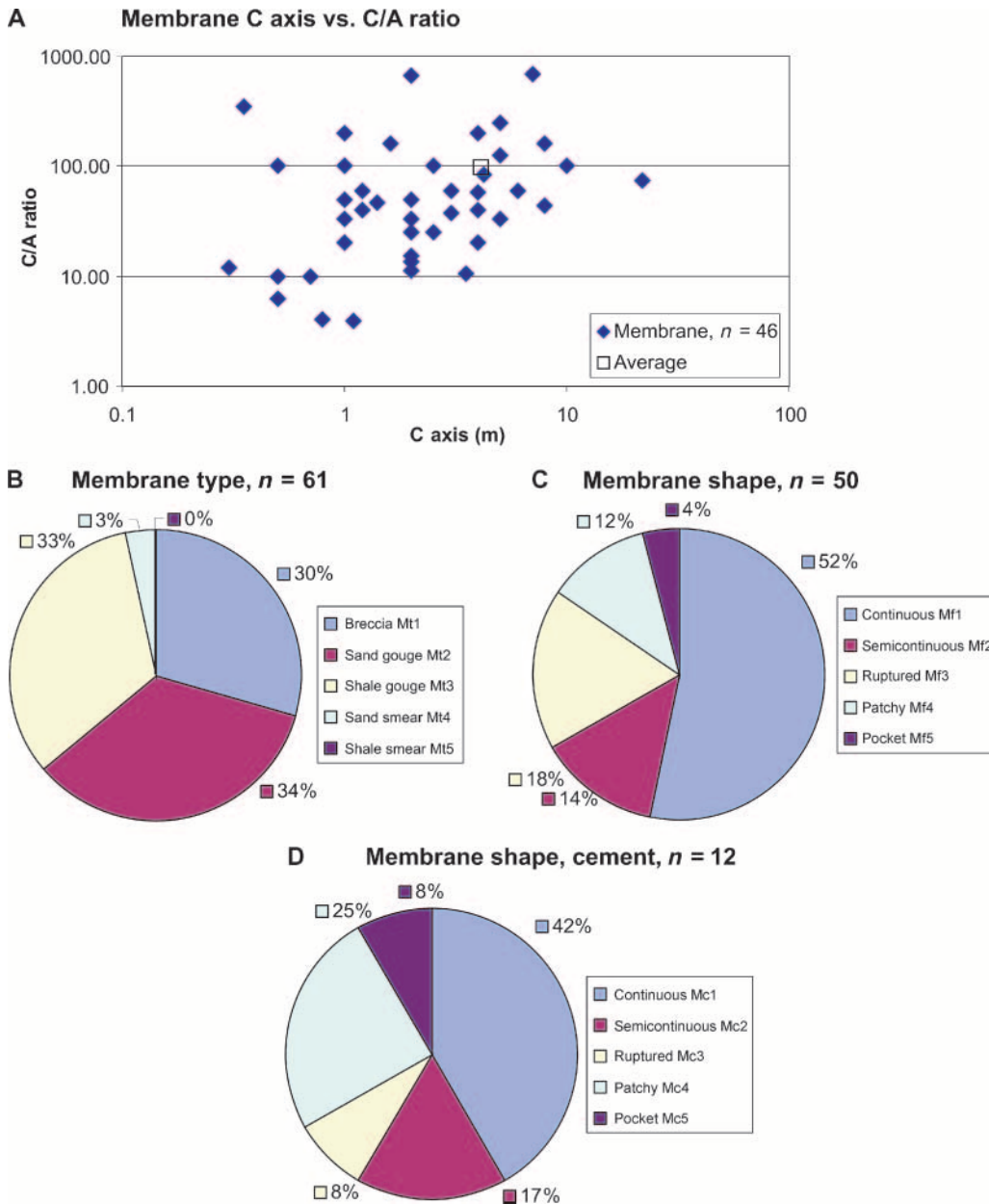
Figure 13. Results from analysis of membranes, shown as percentage of the data set in panels B–D. The classifications used are described in Figure 6. (A) Plot of the long axis of membranes versus the ratio between the long axis and the perpendicular oriented short axis (C/A), both recorded in a vertical section. The average C/A relationship is 100:1. (B) Type of membranes; (C) shape of membranes; (D) shape of cement membranes.

et al., 2006; Wibberley et al., 2008; Childs et al., 2009). An uncertainty in the observed fault thickness is seen because this varies through individual outcrops. The range of thickness (maximum-minimum) plotted against the average thickness shows a general trend; as thickness increases, the range of thickness also increases (Figure 11B). In more detail, the fault statistics show that the fault cores are bound by slip surfaces on the hanging-wall side, in some cases in concert with a surface toward the footwall side (Figure 12). Single slip surfaces dominate, but open networks are observed, similar to those described by Shipton et al. (2005) for sandstones in Utah. The slip surfaces tend to be continuous and parallel to the fault core at the scale of the exposure. Again, the observations are in agreement with other descriptions of slip surfaces (Aydin and Johnson, 1983; Shipton and Cowie, 2001; Davatzes and Aydin, 2003). However, Childs et al. (1997) reported a tendency for fault cores bound by slip surfaces on both sides. This is a subordinate trend in the presented data set because

Figure 14. Results from analysis of lenses, shown as percentage of the data set in panels B–E. The classifications used are described in Figure 7. (A) Plot of the long axis of lenses versus the ratio between the long axis and the perpendicular oriented short axis (C/A), both recorded in a vertical section. The average C/A relationship is approximately 9:1. No obvious trend in the data set is observed. (B) Type of lenses; (C) shape of lenses; (D) type of lenses made up of sandstone; (E) shape of lenses made up of sandstone.
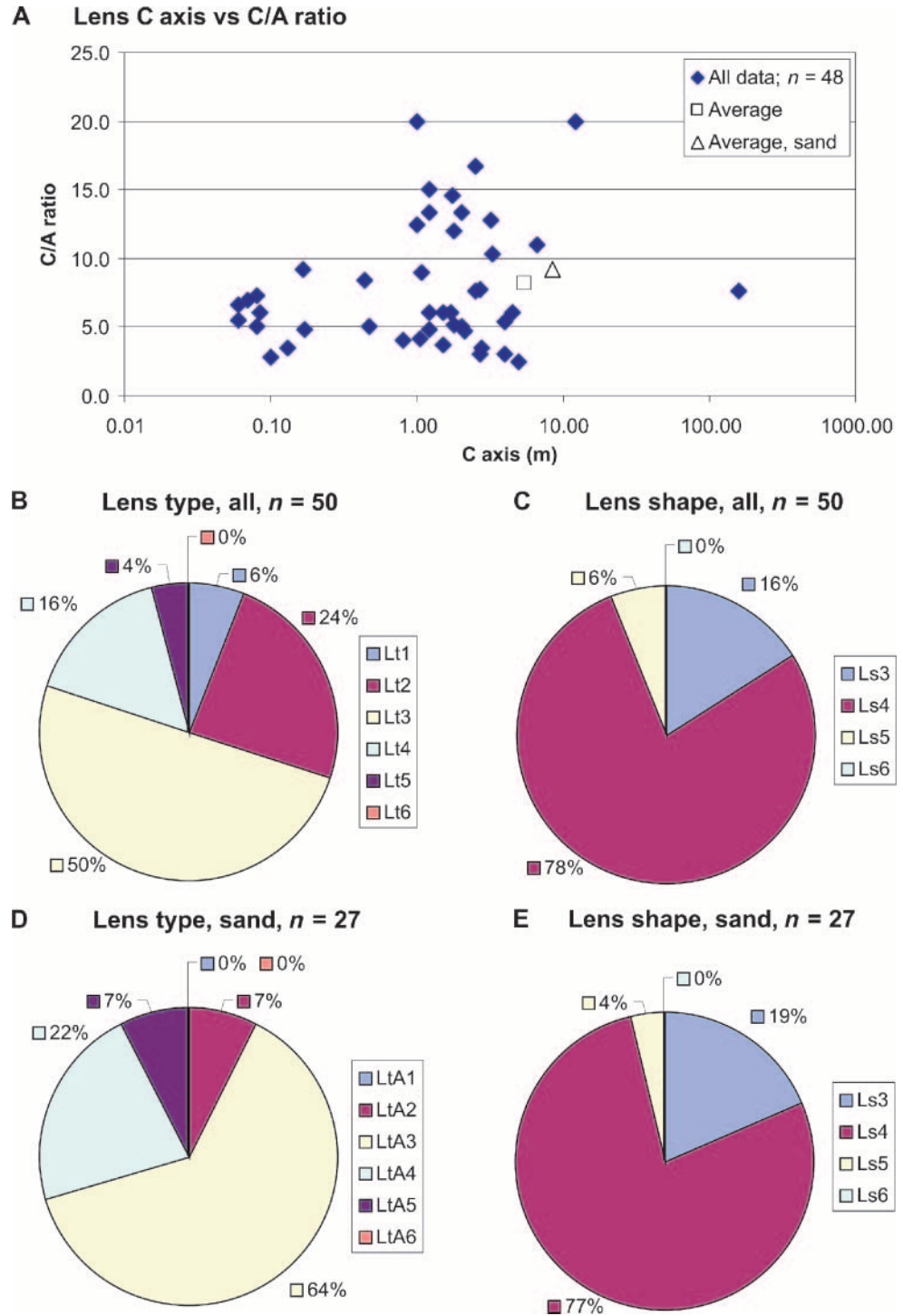
slip surfaces both toward the hanging wall and footwall are found in only 22% of the fault cores. Contrarily, a single principal slip surface at the hanging-wall side of the core is exhibited by 65% of the data set, and in summary, a slip surface toward the hanging wall in 91% of the data set exists.

Membranes are seen as continuous to semicontinuous, long and thin layers of fault rocks, such as sand and shale gouge, and in some cases, breccia (Figure 13). In the literature, only one type of study deals with membrane continuity in a systematic way, the shale smear studies. A commonly reported

number for shale smear along faults is the SSF (Lindsay et al., 1993), equal to the relationship between throw and thickness of the shale source layer. The SSF is highly variable (1–50), but Lindsay et al. (1993) suggested smears to be continuous for factors reaching 7:1 to 11:1. In this interval, the shale membranes are prone to become ruptured (semicontinuous), whereas for lower factors, the shale smear is continuous. Contrarily, Færseth (2006) documented that large faults have ruptured shale smears with SSF as low as 4, and with certain rupture with an SSF of 6. Although such considerations for shale smear can be applied in fault analysis, similar smears are not observed in the presented faults of Sinai. They are characterized by abrasion-type membranes (Yielding et al., 1997), such as shale and sand gouge. This is supported by an average length/thickness ratio that exceeds 100:1, suggesting that they relate to localized zones of concentrated shear or sheared walls to slip surfaces. For sand gouge, this mimics deformation-band cluster zones as, for example, described by Shipton et al. (2005) (see also Aydin and Johnson, 1983; Antonellini and Aydin, 1995; Fossen et al., 2007; Johansen and Fossen, 2008).

Lenses in fault cores are commonly observed in outcrop studies of faults (e.g., Burhannudinnur and Morely, 1997; Childs et al., 1997; Van der Zee and Urai, 2005; Lindanger et al., 2007; Childs et al., 2009). This is in accordance with our data set, in which lenses are observed in 77% of the fault cores (Figure 9). When present, they make up at least half the fault-core area (2-D view) in 64% of the cases; hence they can be considered major constituents of all fault cores. Most observed fault lenses are four sided (Riedel classification of marginal structures). Internally, they reveal fairly intense deformation, dominated by a dense network of shear structures of which many have an R orientation (Figure 14). For sandstone lenses, the pattern is similar, although internal deformation is more prone to be of an open-network type. Internal lens deformation could have several origins (see Lindanger et al., 2007). It could represent damage-zone structures developing before the lens forms and becomes part of the core, either by tip-line bifurcation, segment linkage, splaying, or asperity bifurcation (Childs et al., 1997; Ga-

brielsen and Clausen, 2001; Rykkelid and Fossen, 2002; Childs et al., 2009). It could also represent deformation related to the impact on the lens as the fault reactivates, working toward the breakdown of the lens structure. Another aspect is the shape of lenses. In the presented data set, a significant spread in the long (C) versus short (A) axis ratio is observed, with the average lens C/A ratio being approximately 9:1. In comparison, Lindanger et al. (2007) reported an average C/A ratio of 12.5:1 based on a data set covering both crystalline and sedimentary rocks. However, differences between sites and lithologies are observed, and this variability may explain the discrepancy with our ratio of 9:1. A similar approach to lens description is presented by Antonellini and Aydin (1995), who described the so-called eye structures bound by deformation bands in damage zones of sandstones. Their data on length or wavelength versus width or amplitude gives a power trend through four to five orders of widths. This trend could well describe the pattern of deformation bands and sublenses found internally in the analyzed sandstone lenses of the fault core.

Because the entire data set presented is from one region (western Sinai, Egypt) with certain site-specific characteristics, the statistical trends have limitations in global application. However, they represent guidelines for fault-core characteristics that have significant value as input parameters to fault modeling. To build numerical fault models that render similarity to nature, fault elements have to be quantified. This can be done in deterministic, case true models, or by statistical trend models that acknowledge the uncertainty in the input or outcrop data, as shown by the fault-facies analysis above.

The fault-facies concept is general and therefore valid in all types of fault-rock analyses. However, the most obvious application of the fault-facies approach is within the realm of modeling hydrocarbon and groundwater reservoirs. In reservoir models, each grid cell represents a synthesized or up-scaled version of a more detailed geological reality. Sedimentary facies are currently handled in this way. Faults, however, are merely incorporated as transmissibility multipliers across grid splits and generally without considering the fault impact

within the strain envelope surrounding the fault. The fault-facies approach will allow users to incorporate the full range of elements, geometries, and petrophysical properties present within the fault envelope. This enables users to capture 3-D anisotropic flow inside the deformed rock volume.

The geologists' ultimate goal of presenting the exact fault envelope filled with the correct facies for a given fault in the subsurface will probably never be attained. However, as experience with sedimentary facies modeling shows, this is in many ways not a requirement: using a combination of sensitivity testing and uncertainty analysis, based on extensive databases on sediment distribution and shapes of bodies, one can create models with multiple outcomes that, in detail, clearly are wrong but in summary approximate reality and acknowledge actual uncertainties.

Published data on faults tend to be most concerned with emphasizing heterogeneity instead of looking for similarities and patterns. We envisage that the concept of fault facies may encourage a shift of research toward the identification and quantification of fault-rock properties and patterns of distribution, which are the key for forecasting subsurface reservoir behavior.

REFERENCES CITED

Antonellini, M., and A. Aydin, 1995, Effect of faulting on fluid flow in porous sandstones: Petrophysical properties: AAPG Bulletin, v. 78, p. 355–377.

Arboleya, M. L., and T. Engelder, 1995, Concentrated slip zones with subsidiary shears: Their development on three scales in the Cerro Brass fault zone, Appalachian valley and ridge: Journal of Structural Geology, v. 17, p. 519–532.

Aydin, A., 1978, Small faults formed as deformation bands in sandstone: Pure and Applied Geophysics, v. 116, p. 913–930.

Aydin, A., 2000, Fracture, faults, and hydrocarbon entrapment, migration and flow: Marine and Petroleum Geology, v. 17, p. 79–814.

Aydin, A., and A. M. Johnson, 1983, Analysis of faulting in porous sandstones: Journal of Structural Geology, v. 5, p. 19–31.

Barton, C. C., 1995, Fractal analysis of scaling and spatial clustering of fractures, in C. C. Barton and P. R. La Pointe, eds., Fractals in the earth science: New York, Plenum Press, p. 141–178.

Bastesen, E., A. Braathen, T. Skar, H. Nøttveidt, and R. H.

Gabrielsen, 2009, Extensional fault cores in micritic carbonate—Case studies from the Gulf of Corinth, Greece: Journal of Structural Geology, v. 31, p. 403–421, doi:10.1016/j.jsg.2009.01.005.

Beach, A., A. I. Welborn, P. J. Brockbank, and J. E McCallum, 1999, Reservoir damage around faults: Outcrop examples from the Suez rift: Petroleum Geoscience, v. 5, p. 109–116.

Bense, V. F., E. H. V. d. Berg, and R. T. V. Balen, 2003, Deformation mechanisms and hydraulic properties of fault zones in unconsolidated sediments: The Roer Valley rift system, The Netherlands: Hydrogeology Journal, doi:10.1007/s10040-003-0262-8.

Berg, S. S., and T. Skar, 2005, Controls on damage zone asymmetry of a normal fault zone: Outcrop analyses of a segment of the Moab fault, southeastern Utah: Journal of Structural Geology, v. 27, p. 1803–1822.

Bjørlykke, K., K. Høeg, J. I. Faleide, and J. Jahren, 2005, When do faults in sedimentary basins leak? Stress and deformation in sedimentary basins: Examples from the North Sea and Haltenbanken, offshore Norway: AAPG Bulletin, v. 89, p. 1019–1031.

Boult, P., and J. Kaldi, 2005, Evaluating fault and cap rock seals: AAPG Hedberg Series 2, 268 p.

Braathen, A., P. T. Osmundsen, and R. H. Gabrielsen, 2004, Dynamic development of fault rocks in a crustal-scale detachment: An example from western Norway: Tectonics, v. 23, TC4010, 27 p.

Burhannudinnur, M., and C. K. Morely, 1997, Anatomy of growth fault zones in poorly lithified sandstones and shales: Implications for reservoir studies and seismic interpretation: Part 1. Outcrop study: Petroleum Geoscience, v. 3, p. 211–224.

Caine, J. S., J. P. Evans, and C. B. Forster, 1996, Fault zone architecture and permeability structure: Geology, v. 24, p. 1025–1028.

Chester, F. M., J. P. Evans, and R. L. Biegel, 1993, Internal structure and weakening mechanisms of the San Andreas fault: Journal of Geophysical Research-Solid Earth, v. 98, B1, p. 771–786.

Childs, C., J. Watterson, and J. J. Walsh, 1996, A model for the structure and development of fault zones: Journal of the Geological Society (London), v. 153, p. 337–340.

Childs, C., J. Watterson, and J. J. Walsh, 1997, Complexity in fault zone structure and implications for fault seal prediction: Norwegian Petroleum Society Special Publication 7, p. 61–72.

Childs, C., T. Manzocchi, J. J. Walsh, G. B. Bonson, A. Nicol, M. P. J. Schopfer, 2009, A geometric model of fault zone and fault rock thickness variations: Journal of Structural Geology, v. 31, p. 117–127.

Collettini, C., and R. E. Holdsworth, 2004, Fault zone weakening and character of slip along low-angle normal faults: Insights from the Zuccale fault, Elba, Italy: Journal of the Geological Society (London), v. 161, p. 1039–1051.

Davatzes, N. C., and A. Aydin, 2003, Overprinting faulting mechanisms in high porosity sandstones of southeastern Utah: Journal of Structural Geology, v. 25, p. 1795–1813.

Doughty, P. T., 2003, Clay smear seals and fault sealing potential

of an exhumed growth fault, Rio Grande rift, New Mexico: AAPG Bulletin, v. 87, p. 427–444.

Du Bernard, X., P. Labaume, C. Darcel, P. Davy, and O. Bour, 2002, Cataclastic slip band distribution in normal fault damage zones, Nubian sandstones, Suez rift: Journal of Geophysical Research, v. 107, ETG6-1, p. 6–12.

Ernst, W., 1970, Geochemical facies analysis: Amsterdam, Elsevier Publishing Company, p. 152.

Færseth, R. B., 2006, Shale smear along large faults: Continuity of smear and the fault seal capacity: Journal of the Geological Society (London), v. 163, p. 741–751.

Fossen, H., and J. Hesthammer, 2000, Possible absence of small faults in the Gullfaks field, northern North Sea: Implications for downscaling of faults in some porous sandstones: Journal of Structural Geology, v. 22, p. 851–863.

Fossen, H., R. A. Schultz, K. Mair, and Z. K. Shipton, 2007, Deformation bands in sandstones—A review: Journal of Geological Society (London), v. 164, p. 755–769.

Foxford, K. A., J. J. Walsh, J. Watterson, I. R. Garden, S. C. Guscott, and S. D. Burley, 1998, Structure and content of the Moab fault zone, Utah, U.S.A., and its implications for fault seal prediction, in G. Jones, Q. J. Fisher, and R. J. Knipe, eds., Faulting, fault sealing and fluid flow in hydrocarbon reservoirs: Geological Society (London) Special Publication 147, p. 87–103.

Fredman, N., J. Tveranger, S. L. Semshaug, A. Braathen, and E. Sverdrup, 2007, Sensitivity of fluid flow to fault core architecture and petrophysical properties of fault rocks in siliciclastic reservoirs: A synthetic fault model study: Petroleum Geoscience, v. 13, p. 305–320.

Fredman, N., J. Tveranger, N. Cardozo, A. Braathen, H. Soleng, A. Skorstad, A.-R. Syversveen, and P. Røe, 2008, Assessment of fault facies modeling: Technique and approach for 3D conditioning and modeling of faulted grid: AAPG Bulletin, v. 92, p. 1–20.

Gabrielsen, R. H., and J. A. Clausen, 2001, Horses and duplexes in extensional regimes: A scale-modeling contribution, in H. A. Koyi and N. Mancktelow, eds., Tectonic models: A volume in honor of Hans Ramberg: Geological Society of America Memoir 193, p. 219–233.

Gabrielsen, R. H., R. K. Aarland, and E. Alsaker, 1998, Identification and spatial distribution of fractures in porous, siliclastic sediments, in M. P. Coward, T. S. Daltaban, and H. Johnson, eds., Structural geology in reservoir characterization: Geological Society (London) Special Publication, v. 127, p. 49–56.

Gressly, A., 1838, Observations geologiques sur le Jura Soleurois: Nouve Memoir Society Helvetia Science Naturale (Neuchâtel), v. 2, p. 1–112.

Groshong, R. H., 1975, Strain, fractures and pressure solution in natural single layer folds: Geological Society of America Bulletin, v. 86, p. 1363–1376.

Hancock, P. L., 1985, Brittle microtectonics: Principles and practice: Journal of Structural Geology, v. 7, p. 437–457.

Hansen, E., 1951, Strain facies: New York, Springer-Verlag.

Hesthammer, J., and H. Fossen, 2001, Structural core analysis from the Gullfaks area, northern North Sea: Marine and Petroleum Geology, v. 18, p. 411–439.

Hesthammer, J., P. A. Bjørkum, and L. I. Watts, 2002, The effect of temperature on sealing capacity of faults in sandstone reservoirs: Examples from the Gullfaks and Gullfaks Sør fields, North Sea: AAPG Bulletin, v. 86, p. 1733–1751.

Heynekamp, M. R., L. B. Goodwin, P. S. Mozley, and W. C. Haneberg, 1999, Controls on fault-zone architecture in poorly lithified sediments, Rio Grande rift, New Mexico: Implications for fault-zone permeability and fluid flow, in W. C. Haneberg, P. S. Mozley, J. C. Moore, and L. B. Goodwin, eds., Faults and subsurface fluid flow in the shallow crust: American Geophysical Union Geophysical Monograph 113, p. 27–50.

Huggins, P., J. Watterson, J. J. Walsh, and C. Childs, 1995, Relay zone geometry and displacement transfer between normal faults recorded in coal-mine plans: Journal of Structural Geology, v. 17, p. 1741–1755.

Jamison, W. R., and D. W. Stearns, 1982, Tectonic deformation of Wingate Sandstone, Colorado National Monument: AAPG Bulletin, v. 66, p. 2584–2608.

Johansen, T. E. S., and H. Fossen, 2008, Internal deformation of fault damage zones in interbedded siliciclastic rocks, in C. A. J. Wibberley, W. Kurtz, J. Imber, R. E. Holdsworth, and C. Collettini, eds., The internal structure of fault zones: Implications for mechanical and fluid-flow properties: Geological Society (London) Special Publication 299, p. 35–56.

Katz, Y., R. Weinberger, and A. Aydin, 2004, Geometry and kinematic evolution of Riedel shear structures, Capitol Reef National Park, Utah: Journal of Structural Geology, v. 26, p. 491–501.

Koestler, A. G., and R. Hunsdale, 2002, Hydrocarbon seal quantification: Norwegian Petroleum Society Special Publication 11, 263 p.

Kristensen, M. B., C. J. Childs, and J. A. Korstgård, 2008, The 3D geometry of small-scale relay zones between normal faults in soft sediments: Journal of Structural Geology, v. 30, p. 257–272.

Laubach, S. E., 2003, Practical approaches to identifying sealed and open fractures: AAPG Bulletin, v. 87, p. 561–579.

Laubach, S. E., and M. E. Ward, 2006, Diagenesis in porosity evolution of opening-mod fractures, Middle Triassic to Lower Jurassic La Boca Formation, NE Mexico: Tectonophysics, v. 419, p. 75–97.

Lehner, F. K., and W. F. Pilaar, 1997, The emplacement of clay smears in synsedimentary normal faults: Inferences from field observations near Frechen, Germany, in P. Møller-Pedersen, and A. G. Koestler, eds., Hydrocarbon seals: Importance for exploration and production: Norwegian Petroleum Society Special Publications 7, p. 39–50.

Lindanger, M., R. H. Gabrielen, and A. Braathen, 2007, Analysis of rock lenses in extensional faults: Norwegian Journal of Geology, v. 87, p. 361–372.

Lindsay, N. G., F. C. Murphy, J. J. Walsh, and J. Watterson, 1993, Outcrop studies of shale smears on fault surfaces: Special Publication of the International Association of Sedimentologists 15, p. 113–123.

Logan, J. M., M. Friedman, M. Higgs, C. Dengo, and T. Shimamoto, 1979, Experimental studies of simulated gouge and their application to studies of natural fault zones,

in Analysis of actual fault zones in bedrock: U.S. Geological Survey Open-file Report 79-1239, p. 305–343.

Manzocchi, T., J. J. Walsh, P. Nell, and G. Yielding, 1999, Fault transmissibility multipliers for flow simulation models: Petroleum Geoscience, v. 5, p. 53–63.

Manzocchi, T., A. E. Heath, B. Palananthakumar, C. Childs, and J. J. Walsh, 2008, Faults in conventional flow simulation models: A consideration of representational assumptions and geological uncertainties: Petroleum Geoscience, v. 14, p. 91–110.

Marrett, R., 1996, Aggregate properties of fracture populations: Journal of Structural Geology, v. 18, p. 169–178.

Middleton, G. V., 1978, Facies, *in* R. W. Fairbridge and J. Bougeois, eds., Encyclopedia of sedimentology: Hutchinson & Ross, p. 323–325.

Mitchum Jr., R. M., P. R. Vail, and J. B. Sangree, 1977, Seismic stratigraphy and global changes of sea level: 6. Stratigraphic interpretations of seismic reflection patterns in depositional sequences, *in* C. E. Payton, ed., Seismic stratigraphy—Applications to hydrocarbon exploration: AAPG Memoir 26, p. 117–133.

Moustafa, A. R., 1993, Structural characteristics and tectonic evolution of the east-margin blocks of the Suez rift: Tectonophysics, v. 223, p. 281–299.

Moustafa, A. R., 2004, Geologic maps of the eastern side of the Suez rift (western Sinai Peninsula), Egypt: AAPG Map Series, scale 1:50,000, 9 sheets.

Myers, R., and A. Aydin, 2004, The evolution of faults formed by shearing across joint zones in sandstone: Journal of Structural Geology, v. 26, p. 947–966.

Odling, N. E., 1997, Scaling and connectivity of joint systems in sandstone from western Norway: Journal of Structural Geology, v. 19, p. 1257–1271.

Peacock, D. C. P., 2008, Architecture, gods and gobbledygook: Journal of Structural Geology, v. 30, p. 687–688.

Petit, J. P., 1987, Criteria for the sense of movement on fault surfaces in brittle rocks: Journal of Structural Geology, v. 9, p. 597–608.

Prestholm, E., and O. Walderhaug, 2000, Synsedimentary faulting in a Mesozoic deltaic sequence, Svalbard, Arctic Norway; fault geometries, faulting mechanisms, and sealing properties: AAPG Bulletin, v. 84, p. 505–522.

Rawling, G. C., and L. B. Goodwin, 2006, Structural record of the mechanical evolution of mixed zones in faulted poorly lithified sediments, Rio Grande rift, New Mexico, U.S.A.: Journal of Structural Geology, v. 28, p. 1623–1639.

Reading, H. G., 1986, Sedimentary environments and facies: United Kingdom, Blackwell Scientific Publications, p. 615.

Rider, M., 1996, The geological interpretation of well logs: Latheron, Caithness, United Kingdom, Whittles Publishing, 280 p.

Riedel, W., 1929, Zur mechanic geologischer brucherscheinungnen: Zentralblatt fur Mineralogie, Geologie und Palaeontologie, v. 1929 B, p. 354–368.

Rotevatn, A., H. Fossen, J. Hesthammer, T. E. Aas, and J. A. Howell, 2007, Are relay ramps conduits for fluid flow? Structural analysis of a relay ramp in Arches National Park, Utah: Geological Society (London) Special Publication 270, p. 55–71.

Rotevatn, A., A. Torabi, H. Fossen, and A. Braathen, 2008, Slipped deformation bands: A new type of cataclastic deformation bands in western Sinai, Suez rift, Egypt: Journal of Structural Geology, v. 30, p. 1317–1331.

Rykkelid, E., and H. Fossen, 2002, Layer rotation around vertical fault overlap zones: Observations from seismic data, field examples and physical experiment: Marine and Petroleum Geology, v. 19, p. 181–192.

Schueller, S., A. Braathen, and H. Fossen, 2007, Geometrical characterization of normal fault damage zones in siliciclastic reservoirs (abs.): AAPG and AAPG European Conference, Athens, November 18–21, p. 16.

Schultz, R. A., and H. Fossen, 2008, Terminology for structural discontinuities: AAPG Bulletin, v. 92, p. 853–867.

Schultz, R. A., R. Soliva, H. Fossen, C. H. Okubo, and D. M. Reeves, 2008, Dependence of displacement-length scaling relations for fractures and deformation bands on the volumetric changes across them: Journal of Structural Geology, v. 30, p. 1405–1411.

Seront, B., T. F. Wong, J. S. Caine, C. B. Forster, and R. L. Bruhn, 1998, Laboratory characterization of hydromechanical properties of a seismogenic normal fault system: Journal of Structural Geology, v. 20, p. 865–881.

Sharp, I. R., R. L. Gawthorpe, B. Armstrong, and J. R. Underhill, 2000, Propagation history and passive rotation of mesoscale normal faults: Implications for syn-rift stratigraphic development: Basin Research, v. 12, p. 285–306.

Shipton, Z. K., and P. A. Cowie, 2001, Damage zone and slip-surface evolution over mu m to km scales in highporosity Navajo sandstone, Utah: Journal of Structural Geology, v. 23, p. 1825–1844.

Shipton, Z. K., J. P. Evans, and L. B. Thompson, 2005, The geometry and thickness of deformation-band fault core and its influence on sealing characteristics of deformationband fault zones: AAPG Memoir 85, p. 181–195.

Shipton, Z. K., A. M. Soden, J. D. Kirkpatrick, A. M. Bright, and R. J. Lunn, 2006, How thick is a fault? Fault displacement-thickness scaling revisited: American Geophysical Union, Geophysical Monograph Series 170, p. 193–199.

Sibson, R. H., 1977, Fault rocks and fault mechanisms: Journal of the Geological Society (London), v. 133, p. 191–213.

Soleng, H., A. R. Syversveen, A. Skorstad, and J. Tveranger, 2007, Flow through inhomogeneous fault zones: Society of Petroleum Engineers Paper No. 110331, 9 p.

Sorkhabi, R., and Y. Tsuji, 2005, Faults, fluid flow, and petroleum traps: AAPG Memoir 85, 342 p.

Sperrevik, S., P. A. Gillespie, J. F. Quentin, T. Halvorsen, and R. J. Knipe, 2002, Empirical estimation of fault rock properties, *in* A. G. Koestler and R. Hunsdale, eds., Hydrocarbon seal evaluation: Norwegian Petroleum Society Special Publication 11, p. 109–125.

Steno, N., 1671, Concerning solids naturally contained within solids, Berlin, Springer.

Syversveen, A. R., A. Skorstad, H. H. Soleng, P. Røe, and J. Tveranger, 2006, Facies modeling in fault zones: 10th European Conference on the Mathematics of Oil Recovery, Amsterdam, The Netherlands, September 4–7: Mathematical Geology, v. 38, no. 1, 9 p.

Teichert, C., 1958, Concepts of facies: AAPG Bulletin, v. 42, p. 2718–2744.

Tikoff, B., and H. Fossen, 1999, Three-dimensional reference deformations and strain facies: Journal of Structural Geology, v. 21, p. 1497–1512.

Tveranger, J., A. Braathen, T. Skar, and A. Skauge, 2005, Center for Integrated Petroleum Research—Research activities with emphasis on fluid flow in fault zones: Norwegian Journal of Geology, v. 85, p. 63–72.

Van der Zee, W., and J. L. Urai, 2005, Processes of normal fault evolution in a siliciclastic sequence: a case study from Miri, Sarawak, Malaysia: Journal of Structural Geology, v. 27, p. 2281–2300.

Vermilye, J. M., and C. H. Scholz, 1995, Relation between vein length and aperture: Journal of Structural Geology, v. 17, p. 423–434.

Walderhaug, O., 1996, Kinetic modeling of quartz cementation and porosity loss in deeply buried sandstone reservoirs: AAPG Bulletin, v. 80, p. 731–745.

Walderhaug, O., P. A. Bjørkum, P. H. Nadeau, and O. Langnes, 2001, Quantitative modeling of basin subsidence caused by temperature-driven silica dissolution and precipitation: Petroleum Geoscience, v. 7, p. 107–113.

Wallace, R. E., and H. T. Morris, 1986, Characteristics of faults and shear zones in deep mines: Pageophysics, v. 124, p. 107–125.

Walsh, J., J. Watterson, A. E. Heath, and C. Childs, 1998, Representation and scaling of faults in fluid flow models: Petroleum Geoscience, v. 4, p. 241–251.

Walsh, J. J., W. R. Bailey, C. Childs, A. Nicol, and C. G. Bonson, 2003, Formation of segmented normal faults: A 3-D perspective: Journal of Structural Geology, v. 25, p. 1251–1262.

Wibberley, C. A. J., G. Yielding, and G. Di Toro, 2008, Recent advances in the understanding of fault zone internal structure: A review: Geological Society (London) Special Publication 299, p. 5–33.

Wilson, P., 2008, Comment on "Architecture, gods and gobbledygook": Journal of Structural Geology, v. 30, p. 1614.

Winkler, H. G. F., 1976, Petrogenesis of metamorphic rocks, 4th ed.: New York, Springer-Verlag, 334 p.

Wise, D. U., D. E. Dunn, J. T. Engelder, P. A. Geiser, R. D. Hatcher, S. A. Kish, A. L. Odom, and S. Schamel, 1984, Fault-related rocks; suggestions for terminology: Geology, v. 12, p. 391–394.

Yielding, G., B. Freeman, and D. T. Needham, 1997, Quantitative fault seal prediction: AAPG Bulletin, v. 81, p. 897–917.